Connecting central carbon metabolism, nucleotide metabolism and drug resistance

- A story of pyruvate kinase

By

Fukang She

A dissertation submitted in partial fulfillment of

the requirements for the degree of

Doctor of Philosophy

(Microbiology)

at the

UNIVERSITY OF WISCONSIN-MADISON

2023

Date of final oral examination: 7/27/2023

The dissertation is approved by the following members of the Final Oral Committee:
Jue D. Wang, Professor, Bacteriology
Katrina T. Forest, Professor, Bacteriology
Daniel Amador-Noguez, Associate Professor, Bacteriology
Simon Gilroy, Professor, Botany
Srivatsan Raman, Associate Professor, Biochemistry

Acknowledgements

My graduate school life is fun and fruitful thanks to many people. At first, I would like to thank my PI Jue Wang. She supports my work and exploration even in unfamiliar fields, trains me on thinking about the big picture, and teaches me how to write and present my work to make it easier to understand for the different audience. Her mentoring really helps me to get on the right track for scientific research.

My thesis committee has always been supportive and inspiring. I would like to thank my committee member and collaborator Daniel Amador-Noguez for the brilliant ideas and constant support. He provides professional suggestions on my projects, which largely helps the development of the story. He has introduced many different new technologies to me, which expands my toolbox for research. I am grateful for my committee members Katrina Forest, Simon Gilroy and Vatsan Raman for their thoughtful ideas.

Wang lab alumni and current members have created an awesome environment for scientific research. I would like to thank Brent Anderson. He was a very nice and patient mentor in my early years in research. He helped me to get my hands on experiments, and to get familiar with the English-speaking environment. I would like to thank Jeremy Schroeder. I really enjoyed the time working with Jeremy, we communicated and collaborated on programing. He brought me into the world of microfluidics, and he taught me how to make customed devices for research. And together, we developed the biofilm imaging device, which was an impressive experience. I would like to thank Danny Fung, Jessica Barra, Ponlkrit Yeesin, Christina Giramma, Lucas Onder, Jin Yang, Megan Young, Aude Trinquier, Leah McKinney, Jessie Petrey and McKenna DeFoer for their helps.

I would like to thank all Amador-Noguez lab members for their help with my research. I would like to thank David Stevenson. He helps me on all the HPLC and LCMS related experiments, teaches me relevant knowledge and his experience about LC and MS. These

really helped me to understand the underlying mechanisms of the techniques, and to design the experiments and to analyze the data.

Finally, I would like to thank my parents, my family and all my friends. Life is full of uncertainty; it is all of you that make me who I am today.

Table of Contents

Abstract

Complex metabolism networks allow bacteria to use a large variety of carbon sources from the environment, and the regulation of key nodes in the metabolism network allocates resources to accommodate the changing environment. Pyruvate kinase, the enzyme catalyzes the last step of glycolysis, lies at the junction between glycolysis and the tricarboxylic acid cycle (TCA cycle), a key node in the central carbon metabolism (Figure 1). My thesis reveals previously uncharacterized function and regulation of pyruvate kinase, highlighting the crucial role of regulation of pyruvate kinase in resource allocation. Here using the Gram-positive bacterium *Bacillus subtilis*, we demonstrate that 1) Regulation of pyruvate kinase activity is crucial for the resource partition between glycolysis and the TCA cycle. The resource allocation regulated by pyruvate kinase is important for the resistance to antimicrobial reagents. 2) The alarmone (p)ppGpp regulates the resource partition between nucleotide metabolism and glycolysis.

Firstly, combining *in vitro* enzyme kinetics assay and *in vivo* metabolomics method, we identified an autoinhibitory domain in pyruvate kinase. Lack of this domain led to a constitutively active pyruvate kinase variant. Using the constitutively active pyruvate kinase variant, we showed that pyruvate kinase activity needed to be inhibited or turned off during gluconeogenesis. Failure of inhibition of pyruvate kinase activity resulted in diminished glycolysis intermediates level as biosynthetic precursors. The metabolic defects caused by failure of regulation of pyruvate kinase also led to increased susceptibility to antimicrobial agents that targeted metabolism.

Secondly, we characterized a guanosine toxicity suppressor mutation of *pyk* in a GTP level dysregulated *B. subtilis* strain and revealed that *B. subtilis* pyruvate kinase contributed to a significant part of the synthesis of GTP from GDP, which was important to the viability of the cells under guanosine treatment.

Altogether, our work shed light on the significant roles of pyruvate kinase beyond glycolysis. We revealed that pyruvate kinase is an important GTP producer, and it controls the resource allocation between glycolysis and the TCA cycle, which is crucial for the resistance to antimicrobial reagents.

Chapter 1. Introduction

I. Pyruvate kinase catalyzes a crucial reaction in glycolysis

Utilizing nutrients in the environment to generate biosynthetic precursors and energy for proliferation is the main purpose of metabolism. The ubiquitous pathway glycolysis breaks down glucose to pyruvate, generating glycolytic intermediates which are important precursors for nucleotides and amino acids, as well as energy. Glycolysis usually stands for the Embden–Meyerhof–Parnas (EMP) pathway. Together with the alternative glycolytic pathway Entner–Doudoroff (ED) pathway, they are the primary pathways for glucose breakdown to pyruvate[1]. Both EMP pathway and ED pathway start with the phosphorylation of glucose. In EMP pathway, phosphorylated glucose is isomerized and further phosphorylated before divided into two molecules of triose phosphate. The two molecules of triose phosphate are further converted to two molecules of pyruvate in several steps. While in ED pathway, the phosphorylated glucose is oxidized and isomerized before divided into one molecule of triose phosphate and one molecule of pyruvate. The triose phosphate is then converted to pyruvate in the same way as the EMP pathway.

Pyruvate, the final product of glycolysis, is further fed into the tricarboxylic acid cycle (TCA cycle) and many other pathways to generate more energy and other precursors. Pyruvate kinase is the enzyme that catalyzes the irreversible last step of EMP pathway and ED pathway, transferring the phosphate group from phosphoenolpyruvate (PEP) to ADP, generating one molecule of pyruvate and ATP as the product.

Pyruvate kinase plays an important role in converting PEP to pyruvate. Loss-of-function of pyruvate kinase is lethal during glycolytic growth in many eukaryotes from yeast[2] to human and in some bacteria such as *Staphylococcus aureus*[3], indicating that pyruvate kinase activity is

essential, and no other enzyme can catalyze the conversion of PEP to pyruvate efficiently enough to maintain the growth in those species.

In some other bacterial species such as *Bacillus subtilis*, pyruvate kinase is not essential, but deletion of pyruvate kinase causes severe growth defect. In *B. subtilis*, when pyruvate kinase is absent, part of the PEP is converted to pyruvate by phosphoenolpyruvate: sugar phosphotransferase system (PTS) Enzyme I (E1). And more importantly, the accumulated high PEP level makes PEP carboxykinase (PckA) catalyze the reaction in the direction from PEP to oxaloacetate[4], then pyruvate can be generated from OAA directly or via malate.

However, deletion of pyruvate kinase has been reported to have only minor growth rate change in some bacteria such as *Escherichia coli*[5], likely to be the result of anaplerotic reaction catalyzed by PEP carboxylase, which converts PEP to OAA. While pyruvate kinase is present in most organisms, it is not found in the genome of some bacteria such as *Clostridium thermocellum*. In *C. thermocellum*, the reaction from PEP to pyruvate is catalyzed by pyruvate, phosphate dikinase (PPDK) and through the malate shunt[6].

II. The structure and regulation of pyruvate kinase

The sequence of pyruvate kinase is highly conserved across different kingdoms. Pyruvate kinase monomer usually consists of three domains, A domain is where the active site locates, B domain forms a “lid” above the active site, and C domain contains regulatory ligand binding sites. An addition N-terminal domain is found in some eukaryotic pyruvate kinase, and an extra C-terminal domain is found in pyruvate kinases of some bacteria. Pyruvate kinases usually function as homotetramers with a few exceptions reported.

Enzyme activity of pyruvate kinases are regulated in several different ways. Pyruvate kinases from organisms or tissues with high glycolysis demand are constitutively active, for

example, pyruvate kinase isoform M1 from mammals and pyruvate kinase from *Zymomonas mobilis*. Pyruvate kinases from organisms or tissues capable of doing gluconeogenesis are usually allosterically regulated or regulated by phosphorylation. In rat liver, pyruvate kinase isoform PKL is inactivated via phosphorylation by cAMP dependent protein kinase upon insulin signal. In *E. coli*, two different pyruvate kinases are encoded in the genome. PykA is activated by AMP and PykF is activated by fructose 1,6-bisphosphate. Other allosteric regulators such as fructose 1,6-bisphosphate, AMP, ribose 5-phosphate (R5P), glucose 6-phosphate, and glycerol 3-phosphate are reported in different organisms[3,7–13].

The structural mechanism of pyruvate kinase allosteric regulation is reported in the bacterial pathogen *Mycobacterium tuberculosis*[12] and eukaryotic pathogens *Leishmania mexicana*[14] and *Trypanosoma cruzi*[15]. Upon binding to allosteric activators, pyruvate kinase stays as a tetramer, and the backbone structures of monomers are barely changing, but each monomer is rotating around a central pivot, shifting the inactive tetramer (T-state) to an active tetramer (R-state)[12]. The conformational change of the tetramer is accompanied by the rearrangement of the dimer-dimer interface, where the regulator binding sites locate[12].

Except for the conformational change of tetramer, pyruvate kinase isoform M2 (PKM2) is also regulated by oligomeric state change. Apo PKM2 exists as a mixture of tetramers and monomers, where the equilibrium between tetramer and monomer is controlled by ligand binding. Binding of thyroid hormone triiodothyronine (T3) stabilizes the inactive monomer state, while binding of phenylalanine stabilizes the inactive tetramer state (T-state), and binding of fructose 1,6-bisphosphate stabilizes the active tetramer state (R-state) [16].

III. Pyruvate kinase is involved in various cellular processes beyond the central carbon metabolism

In addition to the crucial role of pyruvate kinase in central carbon metabolism, it also plays important roles in other cellular processes. PKM2 is found in nucleus as well as cytoplasm, suggesting that it has other functions other than catalyzing the metabolic reaction[17]. PKM2 is shown to be a transcriptional coactivator[18] and a protein kinase[19]. Pyruvate kinase from *B. subtilis* is reported to modulate the activity of a lagging-strand DNA polymerase DnaE by direct interaction[20]. *B. subtilis* pyruvate kinase is also reported to play a role in cell division[21].

IV. Reciprocal regulation of glycolysis and gluconeogenesis

Glycolysis breaks down glucose to pyruvate, generating energy and glycolytic intermediates as essential biosynthetic precursors. When sugars are not available, cells consume energy to acquire those essential precursors via gluconeogenesis. Gluconeogenesis operates in the opposite direction of glycolysis, it shares enzymes catalyzing reversible reactions with glycolysis, and using alternative enzymes to bypass irreversible reaction in glycolysis. Therefore, regulation of the glycolysis-specific enzymes and the gluconeogenesis-specific enzymes are required to avoid counteracting reactions.

When enzymes are catalyzing counteracting reactions, the result is usually an energy-consuming cycle without yielding any products. Such cycles are termed futile cycles or substrate cycles. Although futile cycles have been proposed to play roles in heat production[22] and increasing the sensitivity of metabolic control[23], several important steps in glycolysis and gluconeogenesis are regulated to avoid futile cycles.

In the model organism *B. subtilis*, phosphofructokinase (PfkA) is inhibited by PEP, while fructose 1,6- bisphosphatase (Fbp) is inhibited by PEP[24]. During glycolysis, PEP level is

relatively low, resulting in high PfkA activity and low Fbp activity, which is in favor of glycolysis flux; During gluconeogenesis, PEP level is elevated drastically by the inhibition of pyruvate kinase, leading to high Fbp activity and low PfkA activity, which is in favor of gluconeogenic flux.

Except for allosteric regulations, transcriptional regulation also plays a role in the reciprocal regulation of glycolysis and gluconeogenesis. During glycolysis, the gluconeogenesis-specific enzyme PEP carboxykinase (PckA) and gluconeogenesis-specific glyceraldehyde 3-phosphate dehydrogenase (GapB) are transcriptionally repressed by a carbon catabolite control protein CcpN. However, whether and how pyruvate kinase is inhibited during gluconeogenesis in *B. subtilis* is unclear.

V. The alarmone (p)ppGpp: a master regulator of stress response

Bacteria encounter various stresses in diverse environments, making stress response a crucial aspect of their life cycle. (p)ppGpp, an abbreviation for guanosine tetraphosphate and guanosine pentaphosphate, emerges as a significant contributor to bacterial stress response. In response to different stress such as amino acid starvation and antibiotic treatment, (p)ppGpp is synthesized from GTP to modulate multiple cellular processes to cope with the encountered stress. In *Escherichia coli*, (p)ppGpp is synthesized by RelA and SpoT. The major target of (p)ppGpp in *E. coli* is the RNA polymerase and the transcription factor DksA. (p)ppGpp regulates multiple cellular processes via modulating transcription. While in *B. subtilis*, (p)ppGpp is synthesized by RelA, SasA and SasB[25]. Instead of controlling RNA polymerase, (p)ppGpp regulates many targets via direct interaction or via regulating GTP level in *B. subtilis.*

One of the important targets of (p)ppGpp in Gram-positive bacteria is purine nucleotide synthesis. Purine nucleotides are substrates for replication and transcription, provide energy for most energy-consuming reactions in the cell including translation, and also regulate numerous

pathways as allosteric effectors or signaling molecules. Therefore, regulation of purine nucleotide synthesis is of great importance in the growth and proliferation of bacteria.

(p)ppGpp binds to the transcription factor PurR as an anti-inducer to inhibit Pur operon , which encodes the *de novo* purine nucleotide synthesis enzymes[26]. It also directly binds and inhibits purine nucleotide synthesis enzymes like guanylate kinase[27] and the salvage pathway enzyme hypoxanthine phosphoribosyltransferase[28]. In cells lacking RelA, SasA and SasB, (p)ppGpp production is abolished, and the purine synthesis is dysregulated, this can lead to growth arrest or even cell death when extracellular guanosine is added to the media.

VI. (p)ppGpp's role in resource allocation

In general, in both Gram-negative bacteria and Gram-positive bacteria, (p)ppGpp downregulates the synthesis of macromolecules including DNA replication, ribosome RNA transcription, translation and cell wall synthesis[25]. By reducing the production of the macromolecules, bacteria can reserve the resources and re-allocate the resources for stress adaptation. Notably, (p)ppGpp downregulates purine synthesis but upregulates the biosynthesis of amino acids[25]. (p)ppGpp is synthesized from pyrophosphorylation of GTP or GDP by ATP, which are the main purine nucleotides. Therefore, high (p)ppGpp indicates adequate purine nucleotides. However, (p)ppGpp synthesis is induced by amino acid starvation. Thus (p)ppGpp re-allocates the resources from nucleotide synthesis to amino acid synthesis.

VII. Conclusion

In previous works, the regulation and role of pyruvate kinase in glycolysis have been extensively studied. However, there are still open questions: Does the nucleotide diphosphate kinase activity of pyruvate kinase has a physiological role? Is bacterial pyruvate kinase inhibited

during gluconeogenesis? If so, what are the consequences if pyruvate kinase is not properly inhibited during gluconeogenesis? Does pyruvate kinase regulation affect drug resistance?

My thesis work starts from investigating a pyruvate kinase mutant obtained from guanosine toxicity suppressor selection in a (p)ppGpp deficient strain of *B. subtilis* strain. Combining various methods including genetics, enzyme kinetics and metabolomics, I uncovered the roles of pyruvate kinase in nucleotide metabolism, gluconeogenesis and drug resistance. These findings significantly broaden the conventional understanding of pyruvate kinase beyond its recognized role in glycolysis.

1. Sauer, U. & Eikmanns, B. J. The PEP-pyruvate-oxaloacetate node as the switch point for carbon flux distribution in bacteria. *FEMS Microbiol. Rev.* **29**, 765–794 (2005).

2. Ciriacy, M. & Breitenbach, I. Physiological effects of seven different blocks in glycolysis in Saccharomyces cerevisiae. *J. Bacteriol.* **139**, 152–160 (1979).

3. Zoraghi, R. *et al.* Functional Analysis, Overexpression, and Kinetic Characterization of Pyruvate Kinase from Methicillin-Resistant Staphylococcus aureus. *Biochemistry* **49**, 7733–7747 (2010).

4. Zamboni, N., Maaheimo, H., Szyperski, T., Hohmann, H.-P. & Sauer, U. The phosphoenolpyruvate carboxykinase also catalyzes C3 carboxylation at the interface of glycolysis and the TCA cycle of Bacillus subtilis. *Metab. Eng.* **6**, 277–284 (2004).

5. Cunningham, D. S. *et al.* Pyruvate kinase-deficient Escherichia coli exhibits increased plasmid copy number and cyclic AMP levels. *J. Bacteriol.* **191**, 3041–3049 (2009).

6. Olson, D. G. *et al.* Glycolysis without pyruvate kinase in Clostridium thermocellum. *Metab. Eng.* **39**, 169–180 (2017).

7. Waygood, E. B., Rayman, M. K. & Sanwal, B. D. The control of pyruvate kinases of Escherichia coli. II. Effectors and regulatory properties of the enzyme activated by ribose 5-phosphate. *Can. J. Biochem.* **53**, 444–454 (1975).

8. Waygood, E. B. & Sanwal, B. D. The control of pyruvate kinases of Escherichia coli. I. Physicochemical and regulatory properties of the enzyme activated by fructose 1,6-diphosphate. *J. Biol. Chem.* **249**, 265–274 (1974).

9. Sakai, H., Suzuki, K. & Imahori, K. Purification and properties of pyruvate kinase from Bacillus stearothermophilus. *J. Biochem.* **99**, 1157–1167 (1986).

10. Noy, T. *et al.* Central Role of Pyruvate Kinase in Carbon Co-catabolism of Mycobacterium

tuberculosis. *J. Biol. Chem.* **291**, 7060–7069 (2016).

11. Knowles, V. L., Smith, C. S., Smith, C. R. & Plaxton, W. C. Structural and Regulatory Properties of Pyruvate Kinase from the Cyanobacterium Synechococcus PCC 6301 *. *J. Biol. Chem.* **276**, 20966–20972 (2001).

12. Zhong, W. *et al.* Allosteric pyruvate kinase-based “logic gate” synergistically senses energy and sugar levels in Mycobacterium tuberculosis. *Nat. Commun.* **8**, 1986 (2017).

13. Mattevi, A. *et al.* Crystal structure of Escherichia coli pyruvate kinase type I: molecular basis of the allosteric transition. *Structure* **3**, 729–741 (1995).

14. Morgan, H. P. *et al.* Allosteric mechanism of pyruvate kinase from Leishmania mexicana uses a rock and lock model. *J. Biol. Chem.* **285**, 12892–12898 (2010).

15. Morgan, H. P. *et al.* Structures of pyruvate kinases display evolutionarily divergent allosteric strategies. *R. Soc. open Sci.* **1**, 140120 (2014).

16. Morgan, H. P. *et al.* M2 pyruvate kinase provides a mechanism for nutrient sensing and regulation of cell proliferation. *Proc. Natl. Acad. Sci. U. S. A.* **110**, 5881–5886 (2013).

17. Luo, W. *et al.* Pyruvate kinase M2 is a PHD3-stimulated coactivator for hypoxia-inducible factor 1. *Cell* **145**, 732–744 (2011).

18. Luo, W. & Semenza, G. L. Pyruvate kinase M2 regulates glucose metabolism by functioning as a coactivator for hypoxia-inducible factor 1 in cancer cells. *Oncotarget* **2**, 551–556 (2011).

19. Gao, X., Wang, H., Yang, J. J., Liu, X. & Liu, Z.-R. Pyruvate kinase M2 regulates gene transcription by acting as a protein kinase. *Mol. Cell* **45**, 598–609 (2012).

20. Holland, A., Pitoulias, M., Soultanas, P. & Janniere, L. The Replicative DnaE Polymerase

of Bacillus subtilis Recruits the Glycolytic Pyruvate Kinase (PykA) When Bound to Primed DNA Templates. *Life (Basel, Switzerland)* **13**, (2023).

21. Monahan, L. G., Hajduk, I. V, Blaber, S. P., Charles, I. G. & Harry, E. J. Coordinating bacterial cell division with nutrient availability: a role for glycolysis. *MBio* **5**, e00935-14 (2014).

22. Newsholme, E. A. & Crabtree, B. Substrate cycles in metabolic regulation and in heat generation. *Biochem. Soc. Symp.* 61–109 (1976).

23. Newsholme, E. A., Challiss, R. A. J. & Crabtree, B. Substrate cycles: their role in improving sensitivity in metabolic control. *Trends Biochem. Sci.* **9**, 277–280 (1984).

24. Fujita, Y. *et al. Identification and Expression of the Bacillus subtilis Fructose-1,6-Bisphosphatase Gene (fbp)*. *JOURNAL OF BACTERIOLOGY* vol. 180 https://journals.asm.org/journal/jb (1998).

25. Anderson, B. W., Fung, D. K. & Wang, J. D. Regulatory Themes and Variations by the Stress-Signaling Nucleotide Alarmones (p)ppGpp in Bacteria. *Annu. Rev. Genet.* **55**, 115–133 (2021).

26. Anderson, B. W. *et al.* The nucleotide messenger (p)ppGpp is an anti-inducer of the purine synthesis transcription regulator PurR in Bacillus. *Nucleic Acids Res.* **50**, 847–866 (2022).

27. Liu, K. *et al.* Molecular mechanism and evolution of guanylate kinase regulation by (p)ppGpp. *Mol. Cell* **57**, 735–749 (2015).

28. Anderson, B. W. *et al.* Evolution of (p)ppGpp-HPRT regulation through diversification of an allosteric oligomeric interaction. *Elife* **8**, (2019).

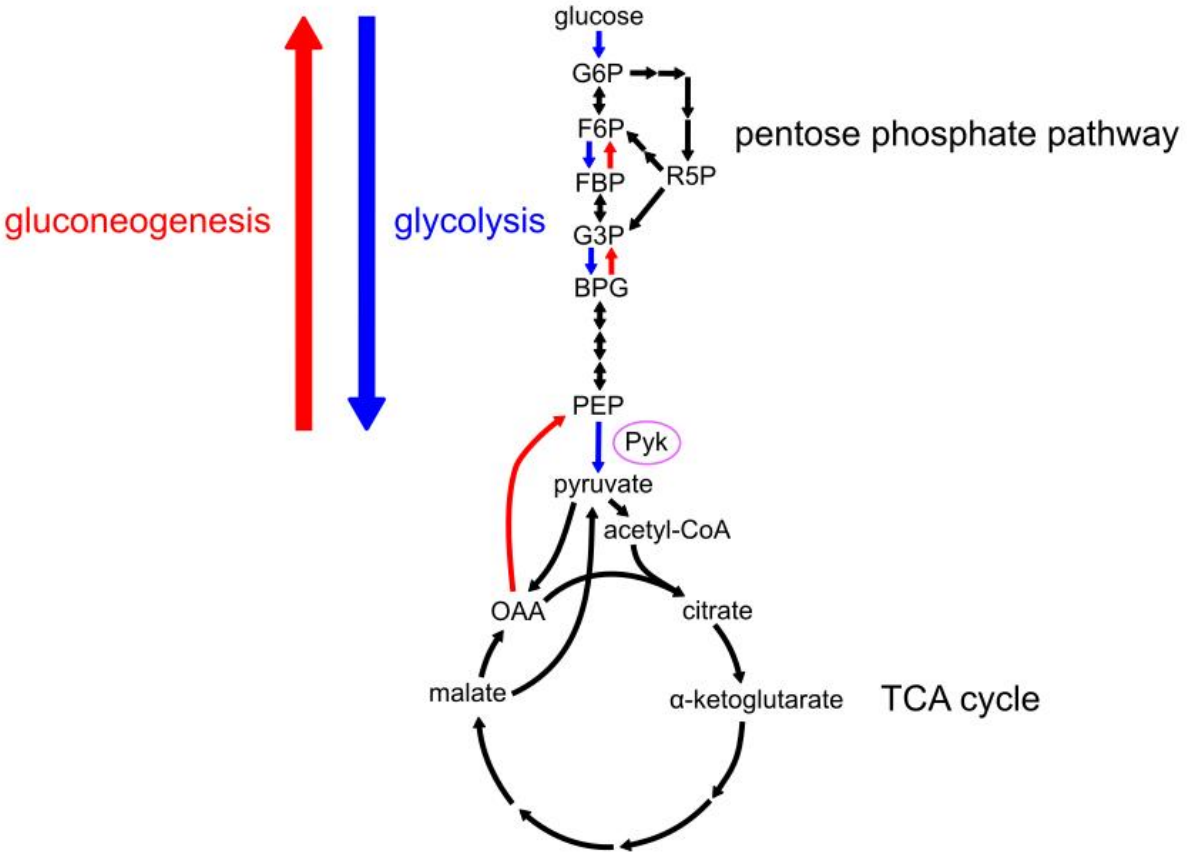

Figure 1. Central carbon metabolism in *B. subtilis*

Schematics of glycolysis, gluconeogenesis, the TCA cycle, and pentose phosphate pathway in *B. subtilis*. Glycolysis and gluconeogenesis specific reactions are colored in blue and red respectively. G6P: glucose 6-phosphate; F6P: fructose 6-phosphate; FBP: fructose 1,6-bisphosphate; G3P: glyceraldehyde 3-phosphate; BPG: 1,3-bisphosphoglycerate; PEP: phosphoenolpyruvate; Pyk: pyruvate kinase; OAA: oxaloacetate; R5P: ribose 5-phosphate.

Chapter 2: Regulation of pyruvate kinase activity prevents metabolic conflicts during gluconeogenesis

Fukang She[1], Brent W. Anderson[1], Shenwei Zhang[2], Wieland Steinchen[3], Danny K. Fung[1], Lauren N. Lucas[1], Nathalie G. Lesser[1], David M. Stevenson[1], Theresa J. Astmann[2], Gert Bange[3], Jan-Peter van Pijkeren[2], Daniel Amador-Noguez[1]*, Jue D. Wang[1]*

[1]University of Wisconsin-Madison, Department of Bacteriology, Madison, USA

[2]University of Wisconsin-Madison, Department of Food Science, Madison, USA

[3]Philipps-University-Marburg, Center for Synthetic Microbiology (SYNMIKRO) & Faculty of Chemistry, Marburg, Germany

Author contributions

F.S., B.W.A., J.D.W. and D.A.N designed the research. F.S., S.Z., W.S., D.K.F., N.G.L., D.M.S. and T.J.A. performed experiments. F.S., S.Z., W.S., D.A.N and J.D.W analyzed data. F.S. wrote the paper. F.S., D.K.F, B.W.A, N.G.L, L.N.L, D.A.N and J.D.W edited the paper.

This chapter is submitted to Nature Chemical Biology.

Abstract

Glycolysis and gluconeogenesis are reciprocal metabolic pathways for utilizing different carbon sources to generate energy and biosynthesis precursors. Pyruvate kinase catalyzes the irreversible last step of glycolysis, but its regulation during gluconeogenesis is poorly understood. Here we found that in the model bacterium *Bacillus subtilis*, pyruvate kinase activity is inhibited during gluconeogenesis, and this regulation requires the pyruvate kinase extra C-terminal domain (ECTD), a conserved domain in Firmicutes. The pyruvate kinase variant lacking ECTD is constitutively active and insensitive to regulatory ligands *in vitro*. Introducing this constitutive pyruvate kinase mutant to *B. subtilis* results in growth defects in gluconeogenic but not glycolytic media and in increased sensitivity to the herbicide glyphosate. We further identified two major metabolic defects due to pyruvate kinase dysregulation during gluconeogenesis: severe depletion of glycolytic intermediates that serve as biosynthetic precursors and inefficient carbon utilization supporting a futile cycle during gluconeogenesis. Our results revealed an allosteric regulation mechanism of pyruvate kinase that is important for the coordination of metabolic flux, for efficient growth, and for antimicrobial resistance.

Introduction

Regulation of central carbon metabolism in microbes allows high efficiency usage of diverse carbon sources[1]. Central carbon metabolism involves glycolysis, gluconeogenesis, the pentose phosphate pathway, and the tricarboxylic acid cycle (TCA cycle). Glycolysis breaks glucose into two molecules of pyruvate, generating energy (ATP) and reducing power (NADH) for oxidative phosphorylation, as well as producing glycolytic intermediates that serve as essential biosynthetic precursors that feed into the pentose phosphate pathway and other pathways for nucleotide and amino acid synthesis. Pyruvate can also feed into the TCA cycle to generate additional reducing power and to replenish biosynthetic precursors. Gluconeogenesis operates in the opposite direction to glycolysis and is required when carbon sources feeding into the early steps of glycolysis are not available. Gluconeogenesis produces essential glycolytic intermediates from non-sugar substrates including organic acids (e.g., malate, succinate, fumarate, pyruvate) and amino acids by consuming energy generated from other pathways.

Gluconeogenesis shares many enzymes that catalyze reversible reactions with glycolysis, and bypasses irreversible reactions with gluconeogenesis-specific enzymes[2] (Figure 1A). How to avoid energy-wasting opposite carbon flows between gluconeogenesis and glycolysis poses a challenge for microorganisms. One strategy is to shut down irreversible glycolysis-specific reactions during gluconeogenesis[3]. The enzyme pyruvate kinase (EC 2.1.7.40) catalyzes the irreversible last step of glycolysis by transferring the phosphate from phosphoenolpyruvate (PEP) to ADP to generate ATP and pyruvate[4]. Pyruvate kinase resides in the metabolic intersection between glycolysis, TCA cycle, and other metabolic pathways, and has been proposed to crosstalk with DNA replication enzymes[5] and cell division in the Gram-positive bacterium *Bacillus subtilis*[6]. Pyruvate kinase has long been proposed to be inhibited during gluconeogenesis[7,8], yet in microbial organisms including *B. subtilis*, pyruvate kinase is not transcriptionally inhibited and remains highly expressed during gluconeogenesis[9]. Bacterial pyruvate kinase is allosterically

regulated by metabolic effectors such as fructose 1,6-bisphosphate[10,11], AMP[11–16], ribose 5-phosphate[11–14] (R5P), glucose 6-phosphate[11,15,16], and glycerol 3-phosphate[11]. However, the molecular mechanisms and the physiological consequences of pyruvate kinase regulation in bacterial species remain incompletely understood.

In this study, we identified a key regulatory function of an extra C-terminal domain (ECTD) of the pyruvate kinases belonging to the bacterial phylum Firmicutes[14,17] and found that it is necessary for allosteric regulation of pyruvate kinase activity. The *B. subtilis* pyruvate kinase ECTD is crucial for the inhibition of its activity during gluconeogenesis, and truncation of this domain produces a constitutively active pyruvate kinase mutant. Using this constitutive mutant, we identified the physiological importance of pyruvate kinase regulation during gluconeogenesis, not just in preventing a futile cycle, but also in maintaining high levels of glycolytic intermediates that serve as essential biosynthetic precursors, the key purpose of gluconeogenesis.

Results

The extra C-terminal domain (ECTD) of pyruvate kinase promotes gluconeogenic growth

Pyruvate kinase is a key glycolytic enzyme that shares conserved architecture of three principal domains (A, B, C domains) from bacteria to eukaryotes (Supplementary Figure 1). In many bacterial species, pyruvate kinase also harbors an extra C-terminal domain (ECTD), which also has had other designations in previous studies (CT[8], ECTS[18], C′ domain[17], PEPut[5]). Phylogenetic analysis of pyruvate kinase sequences from 113 NCBI bacterial reference genomes revealed that pyruvate kinases with an ECTD are conserved in most Firmicutes (except for *Streptococcus* species) and some Cyanobacteria (Figure 1B). Most Firmicutes only have one pyruvate kinase encoded in their genome, while Cyanobacteria usually have two pyruvate kinase isoforms, only one with an ECTD.

We employed the Gram-positive model bacterium *Bacillus subtilis* to investigate the physiological role of the pyruvate kinase ECTD, since this bacterium is a widely studied Firmicute and can utilize a variety of glycolytic and gluconeogenic carbon sources[19]. We engineered a *B. subtilis* mutant (*pykΔectd*) by replacing its wild type *pyk* with a truncated pyruvate kinase retaining residues 1-474 but lacking ECTD at its endogenous locus. We screened phenotypes of this *pykΔectd* mutant on different carbon sources using a Biolog Phenotype MicroArrays which measures cell respiration as a reporter for growth. We found that the *pykΔectd* mutant could utilize the same carbon sources as wild type cells, but for some carbon sources, the mutant displayed different phenotypes. Most notably, the mutant exhibited reduced total cell respiration rates on gluconeogenic carbon sources such as pyruvate and malate but not on glycolytic carbon sources such as glucose and fructose (Supplementary Figure 2). We reasoned that this is because the *pykΔectd* mutant population grew slower specifically during gluconeogenesis, thus resulting in fewer cells than wild type cells. To test this hypothesis, we directly measured the growth curves of *B. subtilis* cells and compared the exponential growth rates of wild type pyruvate kinase (WT), pyruvate kinase deletion (*Δpyk*), and the *pykΔectd* mutant, with either glycolytic (sucrose, glucose, glycerol) or gluconeogenic (pyruvate, malate, alanine) carbon sources (Figure 1C, D). We observed, that during growth in glycolytic carbon sources, there was no difference in growth rate between the wild type and *pykΔectd* strains, while the *Δpyk* mutant grew significantly slower (Figure 1C). This is expected, as pyruvate kinase activity is important for glycolysis. In contrast, during growth in gluconeogenic carbon sources, the *Δpyk* mutant grew similarly to wild type cells, confirming that pyruvate kinase activity is dispensable during gluconeogenesis (Figure 1D). Interestingly, the *pykΔectd* mutant grew significantly slower than both wild type and the *Δpyk* mutant during gluconeogenesis (Figure 1D). While overexpression of wild type *pyk* from an ectopic locus successfully rescued the growth defect of the *Δpyk* mutant (Supplementary Figure 3A), it did not rescue the growth defect of the *pykΔectd* mutant during gluconeogenesis (Supplementary Figure 3B, C). Together these results suggest that *pykΔectd* is a dominant mutant

that likely results in higher or constitutive pyruvate kinase activity than wild type *pyk*. The pyruvate kinase ECTD domain appears to be specifically promoting gluconeogenesis, likely by playing a role in regulation.

To test whether pyruvate kinase ECTD plays a role in gluconeogenesis in Firmicutes beyond *B. subtilis*, we deleted the ECTD domain of pyruvate kinase in the probiotic lactic acid bacterium *Lacticaseibacillus rhamnosus GG*[20]. The resulting *L. rhamnosus GG pykΔectd* mutant grew similarly to wild type cells in glucose medium but displayed a growth defect in pyruvate medium (Figure 1E), suggesting that the pyruvate kinase ECTD domain also promotes gluconeogenic growth in *L. rhamnosus.*

Pyruvate kinase ECTD allows bacterial resistance to the herbicide glyphosate during gluconeogenesis

In addition to growth rate, we also observed a strong effect of pyruvate kinase ECTD in resistance to antimicrobial agent. Glyphosate (the active ingredient of the herbicide Roundup®) is the most commonly used herbicide worldwide[21] and a potent antimicrobial compound[22] that competes with the glycolytic intermediate PEP to inhibit enolpyruvylshikimate 3-phosphate (EPSP) synthase and downstream aromatic amino acid synthesis[23,24] (Supplementary Figure 4A). We examined whether *B. subtilis*, a soil bacterium, could withstand glyphosate-induced toxicity. *B. subtilis* was sensitive to glyphosate when grown in glycolytic media as was reported previously[22], but to our surprise, displayed a much higher resistance to glyphosate when the gluconeogenic substrate malate was supplemented as the sole carbon source (Figure 1F, G). Importantly, the protective effect of gluconeogenesis was strongly dependent on the ECTD domain of the pyruvate kinase, as the minimal inhibitory concentration (MIC) of glyphosate for *pykΔectd* cells was 4-fold lower than that for wild type cells (Figure 1F) and the *pykΔectd* mutant cells displayed strongly reduced growth rates compared to wild type cells in different concentrations of glyphosate (Figure

1G). While wild type cells have high plating efficiency on solid media supplemented with 4.5 mM glyphosate and malate, *pykΔectd* mutant cells form almost no colonies (Figure 1H, Supplementary Figure 4B) except for a single suppressor colony. Genome sequencing of this suppressor pinpointed a single spontaneous mutation: a nucleotide frameshift insertion inside the *pyk* locus causing a premature stop codon in its coding region, which should result in a truncated polypeptide without the active site (Table 1). This observation suggests that loss-of-function of pyruvate kinase suppresses the sensitivity of *pykΔectd* mutant to glyphosate. Thus ECTD allows *B. subtilis* to withstand glyphosate toxicity, likely by enabling negative regulation of pyruvate kinase activity during gluconeogenesis.

The pyruvate kinase ΔECTD mutant has diminished glycolytic intermediates pivotal to gluconeogenesis

Next, we employed LC-MS-based targeted metabolomic analysis to evaluate the activity of pyruvate kinase and central metabolism of *B. subtilis* cells (Figure 2A, Supplementary Figure 5, Supplementary Table 1). We first compared metabolomic profiles of *B. subtilis* wild type cells between glycolysis and gluconeogenesis by providing glucose, malate, or pyruvate as the sole carbon source. We observed large differences in intracellular levels of primary metabolites, highlighting fundamental metabolomic changes between growth in glycolytic and gluconeogenic conditions (Figure 2B, Supplementary Figure 5). Cells grown in glucose had relatively high levels of upper glycolysis intermediates such as G6P and FBP and pentose phosphate pathway intermediates such as R5P and S7P (sedoheptulose 7-phosphate). This can be explained by glucose directly feeding into these pathways. In contrast, cells grown in malate and pyruvate had relatively high levels of lower glycolysis intermediates (e.g. 3PG, BPG, PEP), TCA cycle intermediates (e.g. citrate) and TCA cycle-derived amino acids (e.g. glutamate) compared to cells grown in glucose. This can be explained by malate and pyruvate feeding into the TCA cycle

directly and into lower glycolytic intermediates through PEP. Importantly, the high levels of PEP we observed during gluconeogenesis may facilitate the carbon flux in the reverse direction to glycolysis, allowing cells to generate glycolytic intermediates required for biosynthesis of nucleotides, amino acids, and cell envelop precursors.

To examine how the pyruvate kinase ECTD affects metabolism, we compared the metabolomic profiles of the wild type and *pykΔectd* mutant strains. During glycolytic growth, the key metabolites profiles are similar between wild type and the *pykΔectd* mutant (Supplementary Figure 5). In contrast, during growth on gluconeogenic substrates, the profiles of wild type and mutant are drastically different (Figure 2C, 2D). PEP, the substrate of pyruvate kinase, is depleted by 5-fold to 10-fold in the *pykΔectd* mutant compared to the wild type cells (Figure 2J). Other lower glycolytic intermediates (BPG, 3PG) were similarly depleted during gluconeogenesis, likely because they are derived from PEP through reversible reactions during gluconeogenesis (Figure 2H-I). Upper glycolytic metabolites are also less abundant in *pykΔectd* mutant (Figure 2E), likely a consequence of the depletion of PEP, which is an activator of the gluconeogenesis-specific enzyme fructose 1,6-bisphosphatase[25]. In addition, pentose phosphate pathway intermediates (R5P, S7P) were lower in *pykΔectd* cells than in wild type cells (Figure 2F, 2G), likely a result of decreased levels of glycolytic intermediates that feed into the pentose phosphate pathway. In contrast of these metabolites upstream of pyruvate kinase, the level of amino acids synthesized from pyruvate (alanine and branched-chain amino acids) was higher in *pykΔectd* cells than wild type cells (Figure 2K-2N). These observations suggest a much higher flux through pyruvate kinase in *pykΔectd* cells than in wild type cells during gluconeogenesis, and a consequential failure of generating sufficient glycolytic intermediates for macromolecular biosynthesis.

To directly evaluate the pyruvate kinase activity in the *pykΔectd* mutant during gluconeogenesis, we performed isotope tracing in *B. subtilis* cells. We grew the wild type strain and the *pykΔectd* mutant with [1-^{13}C] pyruvate as the sole carbon source and analyzed the isotope composition of primary metabolites in the cells (Figure 2O, Supplementary Figure 6B). If pyruvate

kinase is inactive, all cellular pyruvate would originate from the external ^{13}C labeled pyruvate source. If pyruvate kinase is active, then pyruvate would also be generated from PEP, which can be produced either from labeled OAA directly from pyruvate or from unlabeled OAA from the TCA cycle. Therefore, pyruvate and its amino acid derivatives should be labeled less with ^{13}C if pyruvate kinase is active. Indeed, we observed a similar proportion of unlabeled PEP in wild type and *pykΔectd* cells (Figure 2P) but a higher proportion of unlabeled pyruvate in *pykΔectd* mutant than in wild type cells (Figure 2Q), supporting the failure of inhibition of pyruvate kinase in the *pykΔectd* mutant. To rule out complications due to pyruvate in the media carried over in the extraction process, we also looked at isotope composition of alanine and valine (Figure 2R, 2S), whose carbon backbones are derived entirely from pyruvate. Both alanine and valine in *pykΔectd* cells also had less ^{13}C labeling than those in wild type cells, confirming that pyruvate kinase in the *pykΔectd* mutant was more active than the wild type pyruvate kinase during gluconeogenic growth, converting PEP to pyruvate and its amino acid derivatives.

Taken together, these results support the idea that wild type pyruvate kinase is inhibited during gluconeogenesis to help build up glycolytic intermediates for anabolism, whereas the pyruvate kinase without ECTD remains active and leads to an impaired metabolome during gluconeogenesis.

Loss of pyruvate kinase ECTD leads to lower carbon use efficiency in gluconeogenesis

Our results indicate that the wild type cells, but not the *pykΔectd* mutant, shut down or strongly inhibit pyruvate kinase activity during gluconeogenesis. In *B. subtilis* and many other bacteria, pyruvate is fed into OAA and back to PEP in two reactions[26]. Therefore, inability to shut down pyruvate kinase during gluconeogenesis would result in an energy-wasting futile cycle with a net of one ATP usage without product accumulation (Figure 3A). Since carbon sources are allocated for energy generation or biosynthesis, if a futile cycle takes place in the cell, a larger

fraction of carbon sources would be consumed for energy generation to compensate for the energy wasted in the futile cycle, leaving a smaller fraction available for making biosynthetic precursors. To test this hypothesis, we grew wild type and *pykΔectd* cells in media with limited amounts (2 g/L) of different carbon sources (glucose, malate, or pyruvate) and measured OD_{600} (optical density at 600 nm) as a proxy for cell growth and biomass accumulation. In glycolytic carbon sources, wild type and *pykΔectd* cells reached similar maximal ODs (Supplementary Figure 7). In gluconeogenic carbon sources, wild type cells reached 25% and 19% higher maximal OD than the *pykΔectd* cells in malate and pyruvate respectively (Figure 3B). This observation suggests that *pykΔectd* cells synthesize biomass less efficiently than wild type cells using gluconeogenic carbon sources.

Failure to reach high OD may be the result of factors other than carbon use efficiency, therefore, we directly quantify carbon use efficiency by measuring the consumption of carbon sources per unit of cell growth. We cultured wild type and *pykΔectd* cells in media with glucose, malate, or pyruvate as the sole carbon source. As cells grew in steady state, we measured the carbon source remaining in the media using HPLC or LC-MS to quantify carbon consumption (Supplementary Figure 8). We found that *pykΔectd* cells utilized glucose as efficiently as wild type but utilized malate and pyruvate significantly less efficiently (Figure 3C). These results confirm that *pykΔectd* cells use gluconeogenic carbon sources less effectively than wild type cells, supporting the existence of a futile cycle during gluconeogenesis.

ECTD is required for the inhibition of *B. subtilis* pyruvate kinase activity *in vitro*

Our *in vivo* results strongly implicate that the pyruvate kinase ECTD is an autoinhibitory domain required for inactivation of pyruvate kinase activity during gluconeogenesis. To examine pyruvate kinase activity *in vitro*, we recombinantly expressed and purified *B. subtilis* wild type pyruvate kinase and a truncated variant without the ECTD (Supplementary Figure 9). Using a gel

filtration assay, we found that both wild type pyruvate kinase and the truncated variant formed the classical homotetramers[8] in solution, indicating the ECTD is not necessary for oligomerization of pyruvate kinase (Figure 4A). We next adapted a classical coupled enzyme assay[27] to measure pyruvate kinase activity in the presence of its potential effectors (Figure 4B). The wild type *B. subtilis* pyruvate kinase activity is inhibited by ATP (Figure 4C) and is activated by AMP and R5P (Figure 4D), known effectors of previously characterized pyruvate kinases from *Geobacillus stearothermophilus*[13] and *Staphylococcus aureus*[14]. In contrast, the pyruvate kinase variant without the ECTD remains enzymatically active but responded to neither the inhibitor ATP nor the activators AMP and R5P (Figure 4E). The modest increase of enzyme activity with ATP is likely to be the result of ADP impurity in ATP.

Pyruvate kinase is well known to exhibit a sigmoidal response to the concentration of the substrate PEP[8]. We therefore evaluated the overall effects by titrating both the substrate PEP and the activator R5P, keeping the inhibitor ATP at a concentration of 5 mM, and quantified their combinational effects on pyruvate kinase activity. The kinetic measurements of wild type *B. subtilis* pyruvate kinase revealed a classical sigmoidal curve for PEP, and activation by R5P (Figure 4F, 4H, Supplementary Table 2). In strong contrast, the truncated enzyme displays a hyperbolic response to PEP and its activity remains high regardless of R5P concentration (Figure 4G, 4I, Supplementary Table 2). Therefore, pyruvate kinase ECTD is crucial for the sigmoidal kinetics to PEP and the inhibition of pyruvate kinase by metabolic effectors such as ATP.

Discussion

Glycolysis and gluconeogenesis are reciprocal central carbon metabolic pathways. Pyruvate kinase carries out the last step of glycolysis by converting the lower glycolytic intermediate PEP to pyruvate. Here we show that pyruvate kinase is shut down during gluconeogenesis to reduce conflict between carbon catabolism and anabolism. Bacteria with

constitutively active pyruvate kinase allele have conflicts between simultaneous glycolytic and gluconeogenic reactions during gluconeogenesis, resulting in growth defects including inefficient carbon usage, slower growth rate, and failure to generate sufficient macromolecular biosynthesis precursors.

Lack of metabolic coordination in the absence of pyruvate kinase regulation also renders bacteria vulnerable to antimicrobials that disrupt cellular metabolism. The herbicide glyphosate attacks the synthesis of aromatic amino acids which uses the glycolytic intermediate PEP as a precursor. The pyruvate kinase constitutive mutant fails to generate high levels of PEP, which can explain its much higher sensitivity to glyphosate. Therefore, regulation of pyruvate kinase is critical for metabolic coordination, with strong impact on carbon efficiency, growth optimization, and resistance to antimicrobial stresses.

While it is clear how the constitutive pyruvate kinase mutant results in metabolic conflict, it is less clear how ECTD enables the regulation of enzyme activity during gluconeogenesis. Pyruvate kinase from many species has been characterized biochemically and has been shown to be allosterically regulated by multiple effectors[10–16,28]. The binding of allosteric effectors leads to the conformational change of the tetramer between inactive “T-state” and active “R-state”[16,29,30]. Pyruvate kinase ECTD interfaces with adjoining monomers in a crystal structure of tetrameric pyruvate kinase[17]. Based on our observations that ΔECTD pyruvate kinase is constitutively active but remains as tetramers, we hypothesize that the ECTD is crucial for keeping the pyruvate kinase tetramer at “T-state”, allowing activation by effectors binding. It is important to note that pyruvate kinases from many bacterial species do not have ECTD, yet they are still allosterically regulated[10,12]. In addition, the pyruvate kinase ECTD is reported to help to maintain thermostability and promote basal pyruvate kinase activities from *Staphylococcus aureus* and *Geobacillus thermophilus*[14,31]. Comparative mechanistic studies of these different pyruvate kinases are needed to yield additional insight into the allosteric regulation of pyruvate kinase.

In addition to mediating allosteric regulation, the ECTD may also undergo phosphorylation, which could contribute to autoinhibition of pyruvate kinase activity. ECTD shares homology with the swiveling domains (Pfam PF00391)[18] of the pyruvate phosphate dikinase and several PEP-utilizing enzymes[32] and contains a conserved active histidine residue that is phosphorylated by PEP or responsible for transferring phosphate group[33–35]. This histidine is conserved in the *B. subtilis* pyruvate kinase ECTD (Supplementary Figure 1)[31] and is a potential phosphorylation site. However, mutation of this histidine to alanine does not change the growth rate in either glycolytic or gluconeogenic media (Supplementary Figure 10). Therefore, phosphorylation on the conserved histidine, if it occurs, is not important for the inhibition of pyruvate kinase during gluconeogenesis. Systematic analyses will help explore the roles of other potential phosphorylation sites on pyruvate kinase[5,36] for their contributions to metabolic regulation.

Pyruvate kinase has been proposed to be inhibited during gluconeogenesis to prevent an energy-wasting futile cycle[8]. However, experimental evidence for this hypothesis has been challenging to obtain due to the lack of a mutant that abolished pyruvate kinase regulation. Here we engineered such a constitutively active mutant in *B. subtilis* and found that its carbon use efficiency under gluconeogenic carbon sources is significantly reduced, which offers strong support for a futile cycle (Figure 3). In *B. subtilis*, pyruvate kinase, pyruvate carboxylase and PEP carboxykinase can form a futile cycle when all enzymes are active (Figure 3A). During glycolysis, the expression of *B. subtilis* PEP carboxykinase is repressed by alternative carbon catabolite repression factor CcpN[37], preventing the futile cycle during glycolysis. During gluconeogenesis, we show that the futile cycle is prevented by ECTD-dependent inhibition of pyruvate kinase activity. Intriguingly, we noticed that, among the 113 bacterial reference genomes, pyruvate carboxylase frequently coexists with the pyruvate kinase ECTD (data not shown). Specifically, most Firmicute species use pyruvate carboxylase with the exception of *Streptococcus* species. *Streptococcus* species, which lack the pyruvate kinase ECTD, employ PEP carboxylase instead of pyruvate carboxylase as an anaplerotic enzyme. As a result, the futile cycle is only between PEP and OAA[38],

and it is not influenced by pyruvate kinase activity (Supplementary Figure 11). Therefore, it is possible that pyruvate kinases in those bacteria are less inhibited during gluconeogenesis. This observation suggests that the pyruvate kinase ECTD possibly evolved to ensure gluconeogenesis efficiency, which allows the efficient utilization of a large variety of carbon sources.

Our results provide strong experimental evidence for existing hypotheses in the literature that the inhibition of pyruvate kinase is important for anabolic metabolism[39]. In mammalian cells, it is proposed that constitutively active pyruvate kinase decreases the carbon flux channeling to biosynthetic pathways for nucleotides and some amino acids[40]. However, depletion of glycolytic intermediates is not directly observed in the mammalian metabolome during glycolytic growth[39]. Here we show with a bacterial model system, that a constitutively active pyruvate kinase does not affect the level of glycolytic intermediates during glycolytic growth but fails to build up high level of glycolytic intermediates during gluconeogenic growth, leading to defective anabolism. Thus, the role of pyruvate kinase regulation for proliferation, irrespective of details, may be conserved from bacteria to human.

Finally, metabolic regulation at the enzymatic activity level is crucial for the fitness of single-cell organisms living in fluctuating nutrient environments. *B. subtilis*, a soil bacterium, utilizes glucose, a glycolytic carbon source, as well as malate, a gluconeogenic carbon source, as its preferred carbon sources[41,42]. Pyruvate kinase activity is crucial in the presence of glucose, but it becomes deleterious in the presence of malate. Inhibition of pyruvate kinase activity removes this deleterious side effect while maintaining high expression of the enzyme, enabling rapid activation of glycolysis upon sensing glycolytic carbon sources. Consequently, inhibiting pyruvate kinase activity via ECTD simultaneously supports efficient gluconeogenesis and facilitates a prompt response to carbon availability and competitive fitness in the changing environment.

Table 1 Strains used in this study

Strain name	Genotype	Reference
DK3287*	*B. subtilis* NCIB3610 Δ*zpdN* ΔSPβ ΔPBSX Δ*comI*	B-E Myagmarjav[43]
JDW3056	DK3287 *pykΔectd*	This work
JDW3420	DK3287*Δpyk*	This work
JDW3955	DK3287 *pyk*^{H539A}	This work
JDW4500	DK3287 *pykΔectd pyk A ins@463*	This work
JDW4328	DK3287 *amyE*::P_{spank}-*pyk*	This work
JDW4330	JDW3056 *amyE*::P_{spank}-*pyk*	This work
JDW4512	JDW3420 *amyE*::P_{spank}-*pyk*	This work
VPL1029	*L. rhamnosus GG*	ATCC 53103
VPL4404	VPL1029 *pykΔectd*	This work

*Referred to as wild type in this paper

Table 2 Plasmids used in this study

Plasmid name	Construct	Purpose	Reference
pJW269	pLIC-trPC-HA	Expression vector	Stols L[44]
pJW422	pLIC-trPC-HA-*pyk*	Expression of *B. subtilis* pyruvate kinase	This work
pJW724	pLIC-trPC-HA-*pykΔectd*	Expression of *B. subtilis* ΔECTD pyruvate kinase	This work
pJW557	pPB41[45] without T7 promoter by the recombination template insertion site	CRISPR editing of genome	Anderson B[46]
pJW693	pJW557 with *pykΔectd* guide RNA and repair template	CRISPR recombineering of *B. subtilis pykΔectd*	This work
pJW442	pJW299[47] with 500 bp upstream and 500 bp downstream sequence of *B. subtilis pyk*	Engineering *B. subtilis Δpyk*	This work
pJW721	pJW557 with *pyk*^{H539A} guide RNA and repair template	CRISPR recombineering of *B. subtilis pyk*^{H539A}	This work
pJW811	pDR110 (from Rudner D) *amyE*::P_{spank}-*B. subtilis pyk*	Express *B. subtilis* pyruvate kinase at non-endogenous site	This work

Materials and Methods

Phylogenetic analysis

For the analysis of distribution of pyruvate kinases containing an ECTD, 118 bacterial reference genomes from the NCBI genome database were compared (Supplementary Table 3). Pyruvate kinase sequences were found in 113 out of 118 reference genomes based on annotations using Biopython[48] and were aligned with MUSCLE in MEGA X[49] using default settings. 16S rRNA sequences from these 113 genomes were identified based on the annotations using Biopython and aligned with ClustalW in MEGA X using default settings. A phylogenetic tree was built with MEGA X using the maximum likelihood method. Data were plotted with R package ggtree[50].

Plasmid and strain construction

For deletion of pyruvate kinase ECTD in *B. subtilis*, Golden Gate Assembly (New England Biolabs) was used to construct a vector with pJW557 (CRISPR/Cas9 vector modified from pPB41[45]) as the backbone. Guide RNAs [oJW3089 (aaacACAGAAGAAGGCGGTTTGACTAGCCATGCTGg) and oJW3090 (aaaacCAGCATGGCTAGTCAAACCGCCTTCTTCTGT)] and the repair template (300 bp upstream and 300 bp downstream of ECTD) were cloned into pJW557. The constructed CRISPR/Cas9 plasmid was transformed into wild type NCIB3610 strain (DK3287) and screened for pyruvate kinase *pykΔectd* mutant by Sanger sequencing.

For the deletion of pyruvate kinase, the plasmid pJW442 was constructed by inserting 500bp upstream and downstream of *pyk* into pEX44[51]. pJW442 was then transformed into DK3287, followed by transformation of I-sceI expression vector pJW296 to induce recombination, and colonies of the Δ*pyk* mutant were purified and confirmed by Sanger sequencing of PCR product.

VPL4404 (*L. rhamnosus GG pykΔectd*) was constructed by homologous recombination using dipeptide ligase as the counterselection marker[52].

Biolog phenotype screening

Wild type and *pykΔectd* mutant were streaked on LB plates and grown overnight at 37°C. Cells were resuspended and diluted to an OD_{600} of 0.007 with inoculation fluid containing redox dye Dye Mix F (Biolog), and then 100 µL culture was inoculated into microplates PM1 and PM2 (Biolog) which contain different carbon sources. Absorbance at 590 nm was monitored by the OmniLog system for 24 hours at 37°C. Data was analyzed using Python and plotted with Matplotlib[53].

***B. subtilis* growth measurement**

For *B. subtilis* growth rate assays, cells were streaked on LB plates and grown at 37°C overnight. 2-3 colonies were resuspended and inoculated into a modified S7 defined media[54] [50 mM MOPS (pH adjusted to 7.0 with KOH), 10 mM $(NH_4)_2SO_4$, 5 mM KH_2PO_4] ($S7_{50}$ minimal media), supplemented with 1% (w/v) carbon source [i.e., glucose, malic acid (pH adjusted to 7 with KOH), sodium pyruvate]. Cells were diluted and grown at 37°C overnight. Before reaching stationary phase, cells were sub-cultured into the same fresh media in 96-well plates with an initial OD_{600} ~0.005, and OD_{600} was monitored by a Synergy 2 microplate reader (BioTek). Data was analyzed using Python and plotted with Matplotlib[53].

For maximum growth density assays, cells were grown in the same way as for growth rate assays above, except that cells were washed with media without a carbon source before inoculation into media with 0.2% (w/v) carbon source to avoid carryover of nutrients.

***L. rhamnosus GG* growth assay**

L. rhamnosus GG wild type and *pykΔectd* cells were inoculated in 5ml De Man, Rogasa and Sharpe (MRS, BD Difco) broth and incubated at 37°C for 16 hours. Overnight cultures were washed twice with modified MRS (10g peptone, 10g beef extract, 5g yeast extract, 2g ammonium citrate dibasic, 0.1g magnesium sulfate, 0.05g manganese sulfate, 2g dipotassium phosphate,

and 1 mL Tween-80, dissolved in water to final volume 900 mL), followed by dilution into fresh mMRS supplemented with either 100 mM glucose, 100 mM of malate, or 100mM of pyruvate to OD_{600} = 0.05. Growth was monitored by a plate reader (Multiskan Sky, Thermo Fisher) at 37°C under hypoxic conditions (5% CO_2, 2% O_2).

Glyphosate resistance assays

For glyphosate resistance assays, cells were grown in the same way as the growth rate assay, except that 0, 0.094, 0.188, 0.375, 0.75, 1.5, 2, 2.5, 3, 4, 5 mM of glyphosate were added to the media. Glyphosate stock solution was made by dissolving glyphosate [N-(phosphonomethyl) glycine] (Sigma-Aldrich) in ddH_2O to 60 mM.

Glyphosate resistance suppressors

JDW4500 was obtained by plating JDW3056 on an agar plate made from $S7_{50}$ minimal media supplemented with 1% (w/v) malic acid (pH adjusted to 7 with KOH), 1.5% (w/v) agar and 4.5 mM glyphosate. A single colony was obtained and verified. Genomic DNA was purified and sent for whole genome sequencing at SeqCenter. Mutation was identified from the sequencing result by breseq[55].

Metabolomic analysis by LC-MS

Cells were grown in the same way as the growth rate assay. Cells from an overnight culture (exponential phase) were inoculated into the same fresh media (50 mM MOPS (pH adjusted to 7.0 with KOH), 10 mM $(NH_4)_2SO_4$, 5 mM KH_2PO_4, and 1% (w/v) carbon source (i.e., glucose, malic acid (pH adjusted to 7 with KOH), sodium pyruvate)) in flasks at an initial OD_{600} ~0.05 and grown to OD_{600} ~0.5. 5 mL of culture were vacuum filtered to collect cells. Filter membranes with cells were submerged in 1.5 mL cold extraction solvent (acetonitrile: methanol: H_2O=40:40:20) over dry ice to quench metabolism. Cell extracts were centrifuged at 13200xg for 10 minutes to remove cell debris. The supernatant was then mixed with an internal control, dried by nitrogen gas flow, and resuspended in HPLC grade H_2O.

For preparation of the internal control, wild type cells were inoculated into media with 50 mM MOPS, 10 mM $(NH_4)_2SO_4$, 5 mM KH_2PO_4, 1% (w/v) [U-^{13}C] glucose, and grown at 37°C. Cells were inoculated into fresh [U-^{13}C] glucose media in flasks at an initial OD_{600} ~0.05 and grown to OD_{600} ~0.5. Metabolites were extracted as described above.

To detect metabolites, samples were analyzed using HPLC-MS consisting of a Dionex UHPLC coupled by electrospray ionization (ESI, negative mode) to a Q Exactive Orbitrap mass spectrometer (Thermo Scientific) operated in full-scan mode for detection of targeted compounds based on their accurate masses. MS parameters were set to a resolution of 70000, an automatic gain control (AGC) of 1e6, a maximum injection time of 40 ms, and a scan range of 70-1000 m/z. LC was performed on an ACQUITY UPLC BEH C18 column (1.7 µm, 2.1 × 100 mm; Waters). Total run time was 25 min with a flow rate of 0.2 mL/min, using 97:3 (v/v) water/methanol, 10 mM tributylamine (pH 8.2-8.5 adjusted with ~9 mM acetic acid) as solvent A and 100% methanol as solvent B. The gradient was as follows: 0 min, 5% B; 2.5 min, 5% B; 17 min, 95% B; 19.5 min, 95% B; 20 min, 5% B; 25 min, 5% B. Raw output data from MS were converted to mzXML format using in-house-developed software, and quantification of metabolites was performed using Metabolomic Analysis and Visualization Engine (MAVEN)[56,57]. Ion counts of metabolites were normalized to OD_{600} and internal controls when applicable. If the ion counts of a metabolite in the internal control was too low, then the ion counts of this metabolite would be normalized to OD_{600} only.

Z scores were calculated within different strains and carbon sources using the formula $Z=(x-\mu)/\sigma$, where x is normalized ion counts, µ is the average of normalized ion counts of a certain metabolite within different conditions, and σ is the standard error of normalized ion counts of a certain metabolite within different conditions.

Carbon use efficiency measurement

For the carbon use efficiency assay, cells were grown in media with $S7_{50}$ minimal media supplemented with 0.2% (w/v) carbon source. As cells were growing, 2 mL of culture were

centrifuged at 16100xg for 1 min to obtain supernatant for carbon source quantification, and 1 mL of culture was collected for OD measurement at each time point.

For quantification of glucose and pyruvate, media samples were mixed with 5 mM [U-^{13}C] glucose or [1-^{13}C] pyruvate as an internal control, and then quantified using LC-MS. MS parameters were set to a resolution of 140000, an automatic gain control (AGC) of 1e6, a maximum injection time of 40 ms, and a scan range of 70-1000 m/z. LC was performed on an ACQUITY UPLC BEH C18 column (1.7 μm, 2.1 × 100 mm; Waters). Total run time was 15 min with a flow rate of 0.2 mL/min, using 97:3 (v/v) water/methanol, 10 mM tributylamine (pH 8.2-8.5 adjusted with ~9 mM acetic acid) as solvent A and 100% methanol as Solvent B. The gradient was as follows: 0 min, 5% B; 2.5 min, 5% B; 7.5 min, 95% B; 9.5 min, 95% B; 10 min, 5% B; 15 min, 5% B.

For quantification of malate, media samples were acidified with 18.4 mM H_2SO_4. After 10 min, samples were centrifuged at 16100 xg for 10 min, and the supernatant was loaded onto the HPLC. LC was performed on a Phenomenex Rezex ROA-Organic Acid H^+ column. Total run time was 45 min with a flow rate of 0.3 mL/min, using 7.6 mM H_2SO_4 as the mobile phase. Refractive index was monitored for the quantification, and concentrations were calculated based on a standard curve generated with 0.8 mM, 4 mM and 20 mM malic acid standards.

Carbon source concentration in the media was plotted versus OD_{600}, displaying a linear correlation. The slope, which was the carbon source consumed per unit of OD_{600}, was used as the indicator of carbon use efficiency.

Protein expression and purification

For pyruvate kinase expression and purification, wild type or ΔECTD pyruvate kinase (Met1 to Asp474) coding sequences were cloned into the pLIC-trPC-HA vector[44] (pJW269) downstream of a sequence encoding the hexa-histidine tag and the tobacco etch virus (TEV) protease cleavage site using ligation independent cloning (LIC)[44].

Wild type and ΔECTD pyruvate kinases were purified as previously described[58]. After purification, enzymes were dialyzed with TEV protease to remove the hexa-histidine tag, and further purified by size-exclusion chromatography. Enzymes were concentrated to ~8 mg/mL, and enzyme concentration was measured by Bradford assay (Bio-Rad). Enzymes were stored in a buffer with 30 mM Tris-HCl (pH=7.5), 100 mM NaCl, 5 mM $MgCl_2$, 25 mM KCl, 1 mM DTT, and 10% (v/v) glycerol before being flash frozen with liquid nitrogen.

Pyruvate kinase kinetics assay

Pyruvate kinase activity was measured by an established coupled-enzyme assay with pyruvate kinase and lactate dehydrogenase[27], in which the product of pyruvate kinase, pyruvate, is used by lactate dehydrogenase to convert NADH to NAD^+. Production of NADH was monitored by the loss of NADH absorbance at 340 nm.

The *B. subtilis* pyruvate kinase reaction mix contained 100 mM Tris-HCl (pH=7.5), 100 mM KCl, 10 mM $MgCl_2$, 1.5 mM PEP (Millipore Sigma), 1 mM ADP (Millipore Sigma), 0.3 mM NADH (Millipore Sigma), and 25 U/mL L-lactate dehydrogenase (from bovine muscle, Millipore Sigma). When indicated, 1 mM AMP (Millipore Sigma) and/or 1 mM R5P (Biosynth International) and/or 5 mM ATP (Millipore Sigma) were added. Enzymatic reactions were initiated by addition of pyruvate kinase to a final concentration of 20 nM, and the absorbance at 340 nm was monitored with a spectrophotometer (Shimadzu UV-2401PC). Data was analyzed using Python and plotted with Matplotlib[53].

For the R5P and PEP titration curve, the reaction mix contained 100 mM Tris-HCl (pH=7.5), 100 mM KCl, 10 mM $MgCl_2$, 0.5 mM ADP, 0.3 mM NADH, 25 U/mL L-lactate dehydrogenase, 5 mM ATP and different concentrations of PEP (0, 0.2, 0.4, 0.6, 0.8, 1.0, 1.2, 1.5 mM) and R5P (0, 20, 40, 60, 80, 100, 200, 300, 400, 500, 600, 700 μM). 4 nM pyruvate kinase was added to the reaction mix to start the reaction, and the absorbance at 340 nm was monitored by a Synergy 2 microplate reader (BioTek). Data were analyzed using Python and plotted with Matplotlib[53]. Wild type pyruvate kinase activity was normalized to the ΔECTD pyruvate kinase activity based on the

maximum velocity, because the purified pyruvate kinase slowly lost activity over the time, and the ΔECTD pyruvate kinase was fresher than the wild type one. Both wild type and the ΔECTD pyruvate kinase kinetics data were fit to an adapted nonessential activation equation[59]:

$$v = \frac{V_{max} * [S]^h}{K_S * \frac{1 + \frac{[A]}{K_A}}{1 + \frac{\beta[A]}{\alpha K_A}} + [S]^h * \frac{1 + \frac{[A]}{\alpha K_A}}{1 + \frac{\beta[A]}{\alpha K_A}}}$$

where [S] represents substrate concentration, [A] represents activator concentration, and h represents the Hill coefficient. Data were fit to the equation above using SciPy[60].

Size exclusion chromatography

100 µl of 100 µM concentrated wild type or ΔECTD pyruvate kinase were applied onto a Superdex200 26/60 GL column (GE Healthcare) and eluted with SEC buffer (20 mM Tris-Cl pH 7.5, 300 mM NaCl, 1 mM EDTA, 1 mM DTT and 10% (v/v) glycerol) at 3 mL/min flow rate at 4 °C. A standard curve for molecular mass determination was obtained using a mixture of thyroglobulin (669 kDa), ferritin (440 kDa), aldolase (158 kDa), conalbumin (75 kDa), ovalbumin (43 kDa), and RNase A (13.7 kDa). The partition coefficient (K_{av}) was calculated as per $K_{av} = (V_e-V_o)/(V_c-V_o)$ with the elution volumes (V_e) of the peak apex of the respective proteins, the given void volume of the column (V_o) of 100 ml and a total column volume (V_c) of 300 ml.

References

1. Buescher, J. M. *et al.* Global network reorganization during dynamic adaptations of Bacillus subtilis metabolism. *Science* **335**, 1099–1103 (2012).

2. Cohen, G. N. Glycolysis, Gluconeogenesis and Glycogen Synthesis BT - Microbial Biochemistry: Second Edition. in (ed. Cohen, G. N.) 63–72 (Springer Netherlands, 2011). doi:10.1007/978-90-481-9437-7_6.

3. Nelson 1942-, D. L. (David L. *Lehninger principles of biochemistry*. (Fourth edition. New York : W.H. Freeman, 2005., 2005).

4. Kayne, F. J. 11 Pyruvate Kinase. in *Group Transfer Part A: Nucleotidyl Transfer Nucleosidyl Transfer Acyl Transfer Phosphoryl Transfer* (ed. Boyer, P. D. B. T.-T. E.) vol. 8 353–382 (Academic Press, 1973).

5. Horemans, S. *et al.* Pyruvate kinase, a metabolic sensor powering glycolysis, drives the metabolic control of DNA replication. *BMC Biol.* **20**, 1–26 (2022).

6. Monahan, L. G., Hajduk, I. V, Blaber, S. P., Charles, I. G. & Harry, E. J. Coordinating bacterial cell division with nutrient availability: a role for glycolysis. *MBio* **5**, e00935-14 (2014).

7. KREBS, H. A. & EGGLESTON, L. V. THE ROLE OF PYRUVATE KINASE IN THE REGULATION OF GLUCONEOGENESIS. *Biochem. J.* **94**, 3C-4C (1965).

8. Enriqueta Muñoz, M. & Ponce, E. Pyruvate kinase: current status of regulatory and functional properties. *Comp. Biochem. Physiol. Part B Biochem. Mol. Biol.* **135**, 197–218 (2003).

9. Nicolas, P. *et al.* Condition-dependent transcriptome reveals high-level regulatory architecture in Bacillus subtilis. *Science* **335**, 1103–1106 (2012).

10. Waygood, E. B. & Sanwal, B. D. The control of pyruvate kinases of Escherichia coli. I. Physicochemical and regulatory properties of the enzyme activated by fructose 1,6-diphosphate. *J. Biol. Chem.* **249**, 265–274

(1974).

11. Knowles, V. L., Smith, C. S., Smith, C. R. & Plaxton, W. C. Structural and Regulatory Properties of Pyruvate Kinase from the Cyanobacterium Synechococcus PCC 6301 *. *J. Biol. Chem.* **276**, 20966–20972 (2001).

12. Waygood, E. B., Rayman, M. K. & Sanwal, B. D. The control of pyruvate kinases of Escherichia coli. II. Effectors and regulatory properties of the enzyme activated by ribose 5-phosphate. *Can. J. Biochem.* **53**, 444–454 (1975).

13. Sakai, H., Suzuki, K. & Imahori, K. Purification and properties of pyruvate kinase from Bacillus stearothermophilus. *J. Biochem.* **99**, 1157–1167 (1986).

14. Zoraghi, R. *et al.* Functional Analysis, Overexpression, and Kinetic Characterization of Pyruvate Kinase from Methicillin-Resistant Staphylococcus aureus. *Biochemistry* **49**, 7733–7747 (2010).

15. Noy, T. *et al.* Central Role of Pyruvate Kinase in Carbon Co-catabolism of Mycobacterium tuberculosis. *J. Biol. Chem.* **291**, 7060–7069 (2016).

16. Zhong, W. *et al.* Allosteric pyruvate kinase-based “logic gate” synergistically senses energy and sugar levels in Mycobacterium tuberculosis. *Nat. Commun.* **8**, 1986 (2017).

17. Suzuki, K., Ito, S., Shimizu-Ibuka, A. & Sakai, H. Crystal structure of pyruvate kinase from Geobacillus stearothermophilus. *J. Biochem.* **144**, 305–312 (2008).

18. Nguyen, C. C. & Saier, M. H. Phylogenetic analysis of the putative phosphorylation domain in the pyruvate kinase of Bacillus stearothermophilus. *Res. Microbiol.* **146**, 713–719 (1995).

19. Saier Jr., M. H. *et al.* Overall Transport Capabilities of Bacillus subtilis. *Bacillus subtilis and Its Closest Relatives* 111–128 (2001) doi:https://doi.org/10.1128/9781555817992.ch10.

20. Doron, S., Snydman, D. R. & Gorbach, S. L. Lactobacillus GG: bacteriology and clinical applications.

Gastroenterol. Clin. North Am. **34**, 483–98, ix (2005).

21. Duke, S. O. & Powles, S. B. Glyphosate: a once-in-a-century herbicide. *Pest Manag. Sci.* **64**, 319–325 (2008).

22. Fischer, R. S., Berry, A., Gaines, C. G. & Jensen, R. A. Comparative action of glyphosate as a trigger of energy drain in eubacteria. *J. Bacteriol.* **168**, 1147–1154 (1986).

23. Fischer, R. S., Rubin, J. L., Gaines, C. G. & Jensen, R. A. Glyphosate sensitivity of 5-enol-pyruvylshikimate-3-phosphate synthase from Bacillus subtilis depends upon state of activation induced by monovalent cations. *Arch. Biochem. Biophys.* **256**, 325–334 (1987).

24. Steinrücken, H. C. & Amrhein, N. The herbicide glyphosate is a potent inhibitor of 5-enolpyruvyl-shikimic acid-3-phosphate synthase. *Biochem. Biophys. Res. Commun.* **94**, 1207–1212 (1980).

25. Fujita, Y. & Freese, E. Purification and properties of fructose-1,6-bisphosphatase of Bacillus subtilis. *J. Biol. Chem.* **254**, 5340–5349 (1979).

26. Sauer, U. & Eikmanns, B. J. The PEP-pyruvate-oxaloacetate node as the switch point for carbon flux distribution in bacteria. *FEMS Microbiol. Rev.* **29**, 765–794 (2005).

27. Kornberg, A. & Pricer, W. E. ENZYMATIC PHOSPHORYLATION OF ADENOSINE AND 2,6-DIAMINOPURINE RIBOSIDE. *J. Biol. Chem.* **193**, 481–495 (1951).

28. Mattevi, A. *et al.* Crystal structure of Escherichia coli pyruvate kinase type I: molecular basis of the allosteric transition. *Structure* **3**, 729–741 (1995).

29. Morgan, H. P. *et al.* Allosteric mechanism of pyruvate kinase from Leishmania mexicana uses a rock and lock model. *J. Biol. Chem.* **285**, 12892–12898 (2010).

30. Morgan, H. P. *et al.* M2 pyruvate kinase provides a mechanism for nutrient sensing and regulation of cell

proliferation. *Proc. Natl. Acad. Sci. U. S. A.* **110**, 5881–5886 (2013).

31. Sakai, H. Possible structure and function of the extra C-terminal sequence of pyruvate kinase from Bacillus stearothermophilus. *J. Biochem.* **136**, 471–476 (2004).

32. Pocalyko, D. J., Carroll, L. J., Martin, B. M., Babbitt, P. C. & Dunaway-Mariano, D. Analysis of sequence homologies in plant and bacterial pyruvate phosphate dikinase, enzyme I of the bacterial phosphoenolpyruvate: sugar phosphotransferase system and other PEP-utilizing enzymes. Identification of potential catalytic and regulatory motif. *Biochemistry* **29**, 10757–10765 (1990).

33. Lim, K. *et al.* Swiveling domain mechanism in pyruvate phosphate dikinase. *Biochemistry* **46**, 14845–14853 (2007).

34. Teplyakov, A. *et al.* Structure of phosphorylated enzyme I, the phosphoenolpyruvate:sugar phosphotransferase system sugar translocation signal protein. *Proc. Natl. Acad. Sci. U. S. A.* **103**, 16218–16223 (2006).

35. Herzberg, O. *et al.* Swiveling-domain mechanism for enzymatic phosphotransfer between remote reaction sites. *Proc. Natl. Acad. Sci. U. S. A.* **93**, 2652–2657 (1996).

36. Eymann, C. *et al.* Dynamics of protein phosphorylation on Ser/Thr/Tyr in Bacillus subtilis. *Proteomics* **7**, 3509–3526 (2007).

37. Tännler, S. *et al.* CcpN controls central carbon fluxes in Bacillus subtilis. *J. Bacteriol.* **190**, 6178–6187 (2008).

38. Xu, Y.-F., Amador-Noguez, D., Reaves, M. L., Feng, X.-J. & Rabinowitz, J. D. Ultrasensitive regulation of anapleurosis via allosteric activation of PEP carboxylase. *Nat. Chem. Biol.* **8**, 562–568 (2012).

39. Israelsen, W. J. & Vander Heiden, M. G. Pyruvate kinase: Function, regulation and role in cancer. *Semin.*

Cell Dev. Biol. **43**, 43–51 (2015).

40. Lunt, S. Y. *et al.* Pyruvate kinase isoform expression alters nucleotide synthesis to impact cell proliferation. *Mol. Cell* **57**, 95–107 (2015).

41. Meyer, F. M. & Stülke, J. Malate metabolism in Bacillus subtilis: Distinct roles for three classes of malate-oxidizing enzymes. *FEMS Microbiol. Lett.* **339**, 17–22 (2013).

42. Rudrappa, T., Czymmek, K. J., Paré, P. W. & Bais, H. P. Root-secreted malic acid recruits beneficial soil bacteria. *Plant Physiol.* **148**, 1547–1556 (2008).

43. Myagmarjav, B.-E., Konkol, M. A., Ramsey, J., Mukhopadhyay, S. & Kearns, D. B. ZpdN, a Plasmid-Encoded Sigma Factor Homolog, Induces pBS32-Dependent Cell Death in Bacillus subtilis. *J. Bacteriol.* **198**, 2975–2984 (2016).

44. Stols, L. *et al.* A new vector for high-throughput, ligation-independent cloning encoding a tobacco etch virus protease cleavage site. *Protein Expr. Purif.* **25**, 8–15 (2002).

45. Burby, P. E. & Simmons, L. A. CRISPR/Cas9 Editing of the Bacillus subtilis Genome. *Bio-protocol* **7**, e2272 (2017).

46. Anderson, B. W. *et al.* The nucleotide messenger (p)ppGpp is an anti-inducer of the purine synthesis transcription regulator PurR in Bacillus. *Nucleic Acids Res.* **50**, 847–866 (2022).

47. Liu, K. *et al.* Molecular mechanism and evolution of guanylate kinase regulation by (p)ppGpp. *Mol. Cell* **57**, 735–749 (2015).

48. Cock, P. J. A. *et al.* Biopython: freely available Python tools for computational molecular biology and bioinformatics. *Bioinformatics* **25**, 1422–1423 (2009).

49. Kumar, S., Stecher, G., Li, M., Knyaz, C. & Tamura, K. MEGA X: Molecular Evolutionary Genetics Analysis

across Computing Platforms. *Mol. Biol. Evol.* **35**, 1547–1549 (2018).

50. Yu, G., Smith, D. K., Zhu, H., Guan, Y. & Lam, T. T.-Y. ggtree: an r package for visualization and annotation of phylogenetic trees with their covariates and other associated data. *Methods Ecol. Evol.* **8**, 28–36 (2017).

51. Comella, N. & Grossman, A. D. Conservation of genes and processes controlled by the quorum response in bacteria: characterization of genes controlled by the quorum-sensing transcription factor ComA in Bacillus subtilis. *Mol. Microbiol.* **57**, 1159–1174 (2005).

52. Zhang, S., Oh, J.-H., Alexander, L. M., Özçam, M. & van Pijkeren, J.-P. d-Alanyl-d-Alanine Ligase as a Broad-Host-Range Counterselection Marker in Vancomycin-Resistant Lactic Acid Bacteria. *J. Bacteriol.* **200**, (2018).

53. Hunter, J. D. Matplotlib: A 2D Graphics Environment. *Comput. Sci. Eng.* **9**, 90–95 (2007).

54. Vasantha, N. & Freese, E. Enzyme changes during Bacillus subtilis sporulation caused by deprivation of guanine nucleotides. *J. Bacteriol.* **144**, 1119–1125 (1980).

55. Deatherage, D. E. & Barrick, J. E. Identification of mutations in laboratory-evolved microbes from next-generation sequencing data using breseq. *Methods Mol. Biol.* **1151**, 165–188 (2014).

56. Clasquin, M. F., Melamud, E. & Rabinowitz, J. D. LC-MS data processing with MAVEN: a metabolomic analysis and visualization engine. *Curr. Protoc. Bioinforma.* **Chapter 14**, Unit14.11 (2012).

57. Melamud, E., Vastag, L. & Rabinowitz, J. D. Metabolomic analysis and visualization engine for LC-MS data. *Anal. Chem.* **82**, 9818–9826 (2010).

58. Anderson, B. W. *et al.* Evolution of (p)ppGpp-HPRT regulation through diversification of an allosteric oligomeric interaction. *Elife* **8**, (2019).

59. Segel, I. H. *Enzyme kinetics : behavior and analysis of rapid equilibrium and steady state enzyme systems* . (Wiley, 1993).

60. Virtanen, P. *et al.* SciPy 1.0: fundamental algorithms for scientific computing in Python. *Nat. Methods* **17**, 261–272 (2020).

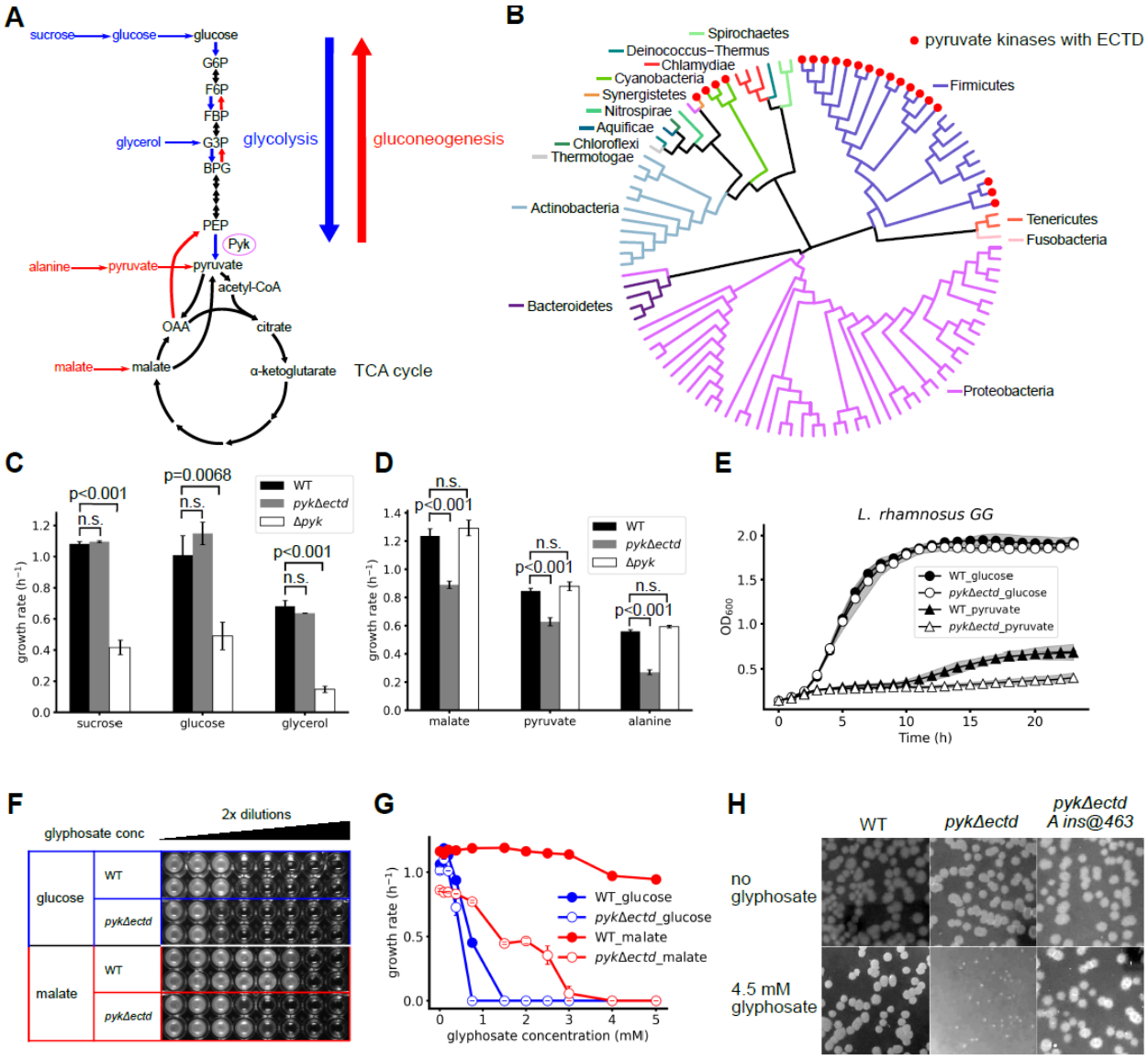

Fig 1. Loss of pyruvate kinase ECTD leads to growth defects and hypersensitivity to glyphosate in gluconeogenic carbon sources

(A) Diagram of glycolysis and the TCA cycle, showing glycolytic and gluconeogenic specific reactions in blue and red, respectively. Glycolytic and gluconeogenic carbon sources used in growth assays are labeled in blue and red respectively. G6P: glucose 6-phosphate; F6P: fructose 6-phosphate; FBP: fructose 1,6-bisphosphate; G3P: glyceraldehyde 3-phosphate; BPG: 1,3-bisphosphoglycerate; Pyk: pyruvate kinase. (B) Phylogenetic tree that shows the distribution of pyruvate kinase ECTD in 113 bacterial reference genomes. (C)-(D) Growth rates of wild type,

pykΔectd, and *Δpyk* cells in media with (C) glycolytic or (D) gluconeogenic sole carbon sources. F test is performed for each group, followed by Tukey's HSD test. p values of Tukey's HSD test are labeled in the figure if smaller than 0.05; p values larger than 0.05 are labeled as n.s. (not significant). (E) Growth curves of *L. rhamnosus GG* wild type strain and *pykΔectd* mutant in media supplemented with glucose or pyruvate as carbon source. Gray region represents 95% confidence interval. (F) Minimal inhibitory concentration (MIC) of glyphosate for wild type and *pykΔectd* cells in glycolytic or gluconeogenic media. Glyphosate concentrations were 0.1875, 0.375, 0.75, 1.5, 3, 6, 12, 24 mM from left to right. (G) Growth rate of wild type and *pykΔectd* strains in media with glucose or malate as the sole carbon source under different concentrations of glyphosate. Error bars represent standard error of the mean of duplicates. (H) Colony images of wild type, *pykΔectd*, and the glyphosate suppressor on malate minimal plates with or without glyphosate.

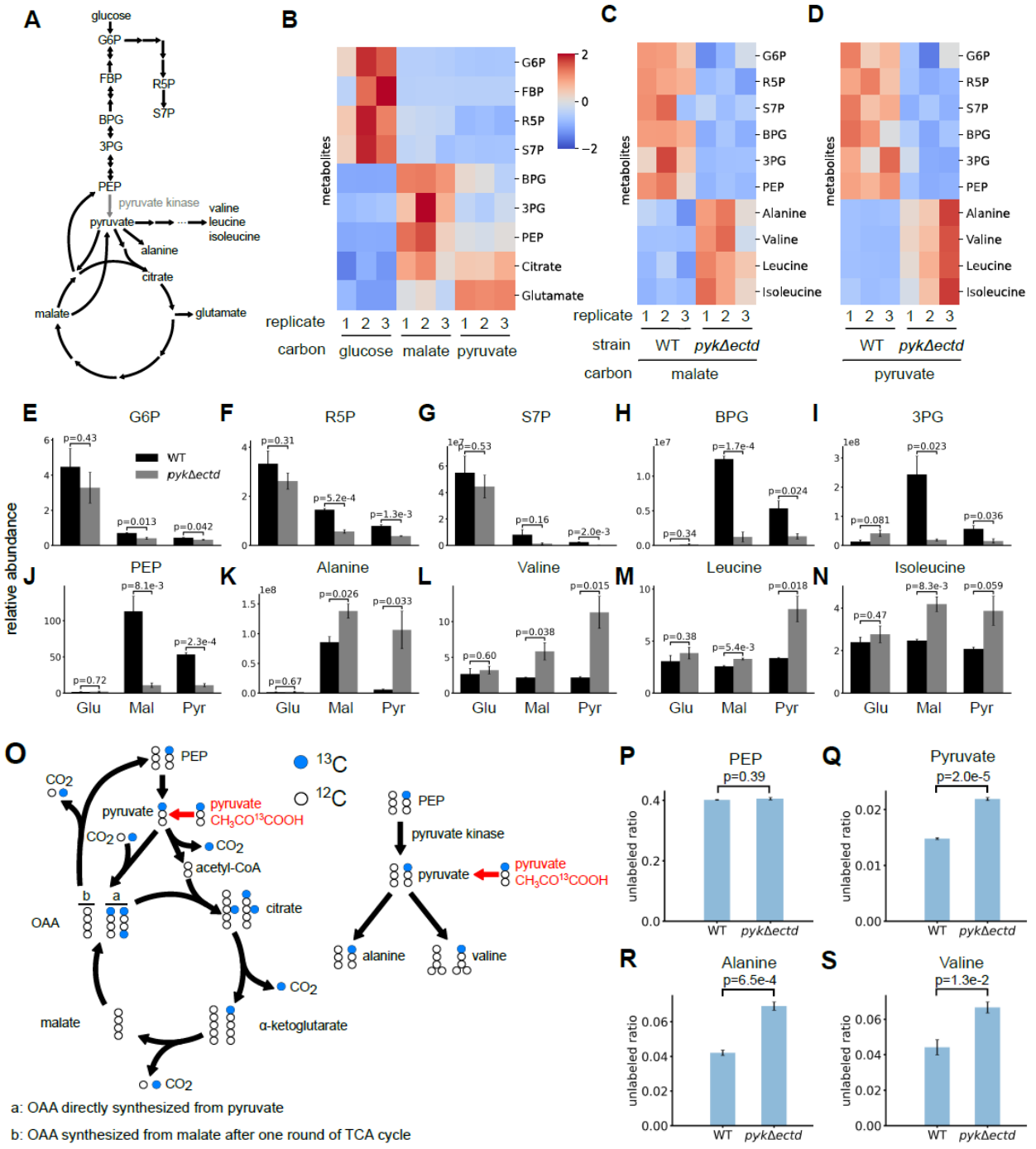

Fig 2. Loss of pyruvate kinase ECTD leads to depletion of glycolysis intermediates during gluconeogenesis

(A) Schematics of gluconeogenesis, part of the pentose phosphate pathway, and the TCA cycle. Important target metabolites are indicated. G6P: glucose 6-phosphate; FBP: fructose 1,6-bisphosphate; R5P: ribose 5-phosphate; S7P: sedoheptulose 7-phosphate; BPG: 1,3-

bisphosphoglycerate; 3PG: 3-phosphoglycerate. (B) Levels of metabolites in wild type cells grown in glycolytic or gluconeogenic carbon sources. (C)-(D) Comparison of levels of metabolites in wild type and *pykΔectd* cells grown in gluconeogenic carbon sources (C) malate and (D) pyruvate. (E)-(N) Relative abundance of metabolites upstream and downstream of pyruvate kinase. Relative abundances are calculated based on internal control, except for S7P, BPG, 3PG and alanine. See Materials and Methods: Metabolic analysis by LC-MS. (O) Schematics of labeling of major metabolites in cells grown with [1-^{13}C] pyruvate. (P)-(S) Unlabeled ratio of PEP, pyruvate, alanine and valine in wild type and *pykΔectd* cells grown in media with [1-^{13}C] labeled pyruvate as the sole carbon source.

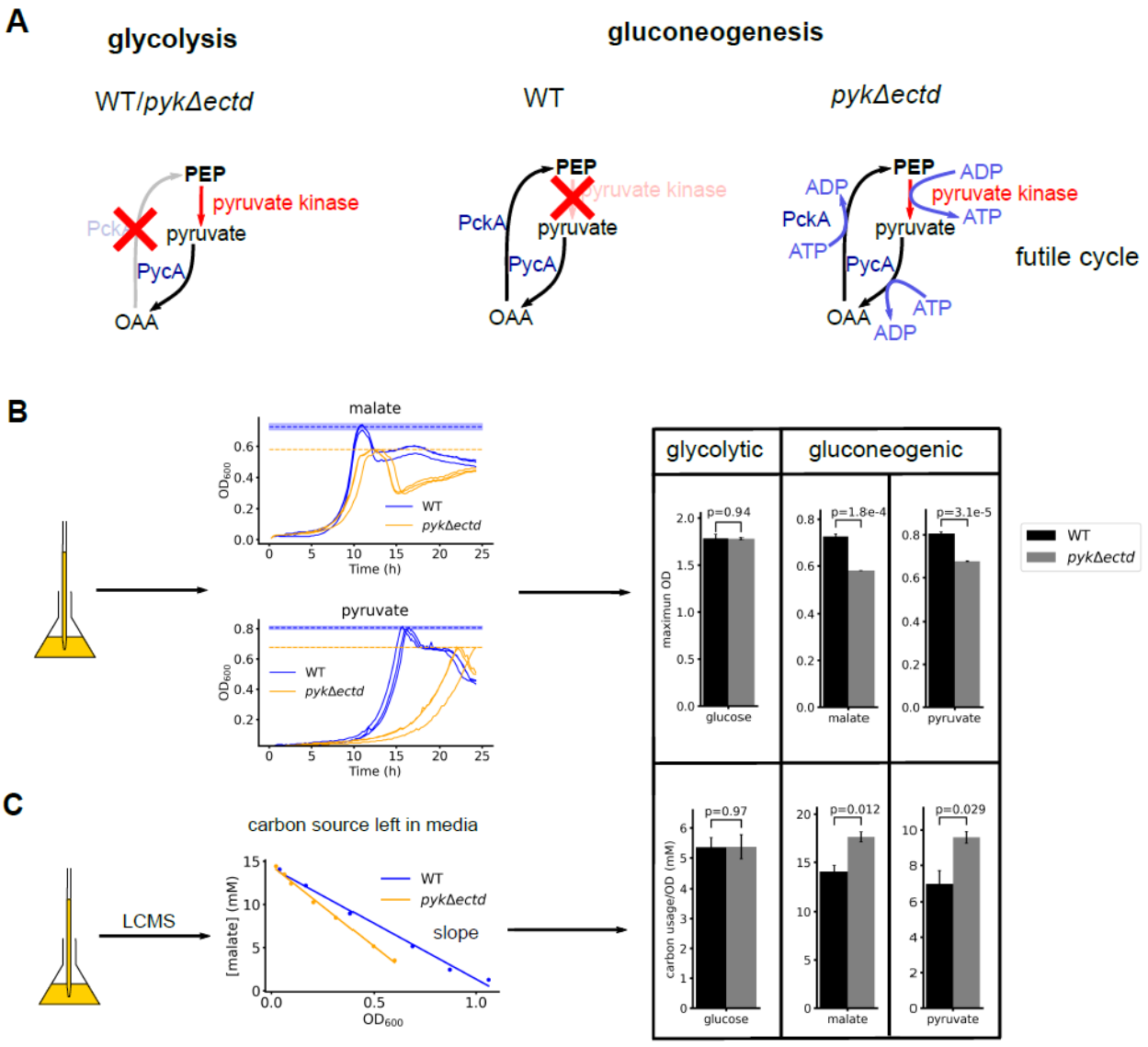

Fig 3. Loss of pyruvate kinase ECTD leads to energy waste and low carbon use efficiency during gluconeogenesis

(A) Schematics of the futile cycle model. Presumably, in *pykΔectd* cells during gluconeogenic growth, pyruvate kinase, pyruvate carboxylase and PEP carboxykinase are active simultaneously. The three reactions form a futile cycle that consumes one molecule of ATP every cycle without product accumulation. PycA: pyruvate carboxylase; PckA: PEP carboxykinase. (B) Maximum OD_{600} of wild type or *pykΔectd* cells grown in media with 2 g/L of different sole carbon sources. Dashed lines represent the average maximum ODs for each condition, colored region represents

95% confidence interval. (C) Carbon source usage per OD_{600} increase for wild type and *pykΔectd* cells in media with different sole carbon sources.

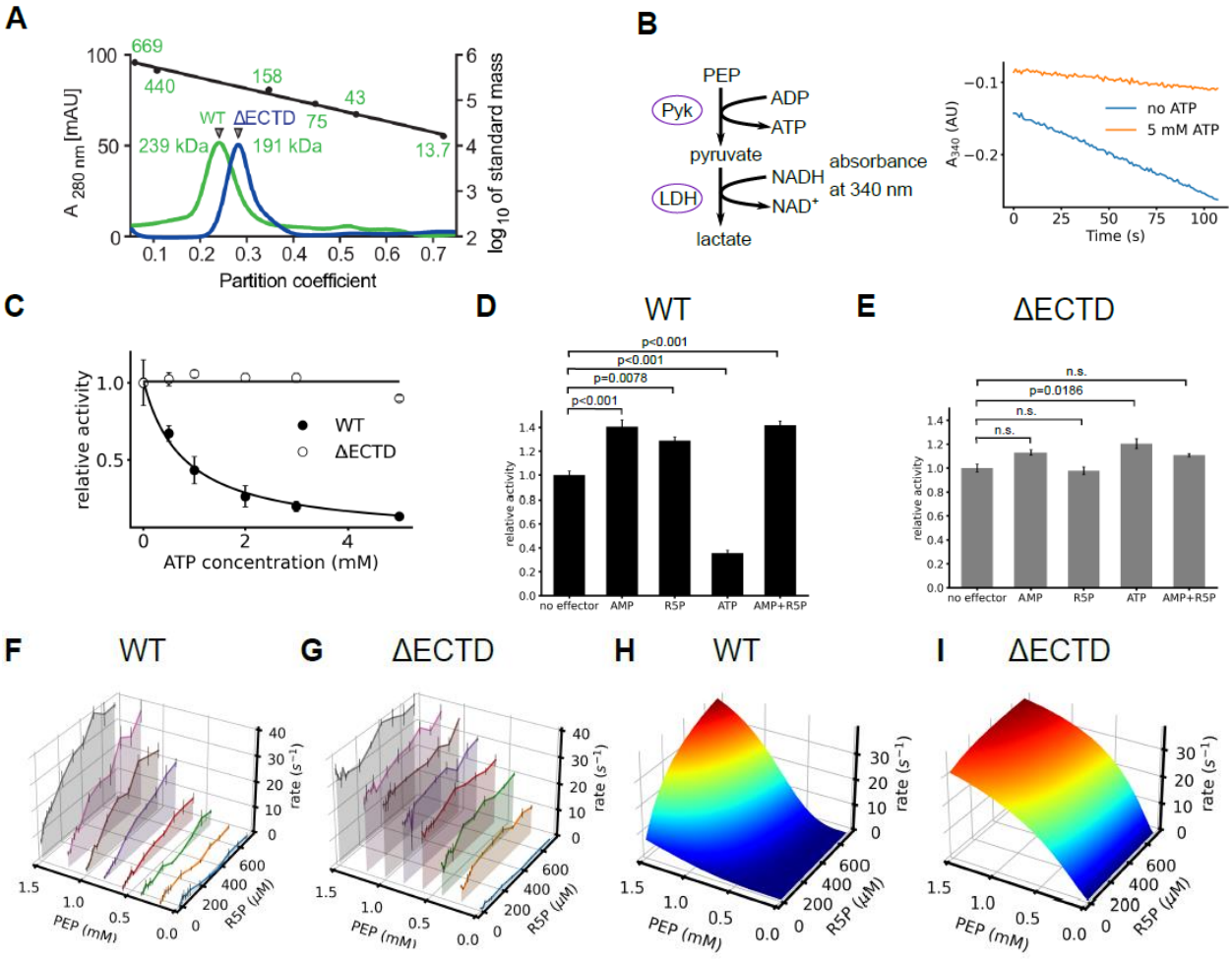

Fig 4. Pyruvate kinase ECTD is required for the inhibition of pyruvate kinase activity at low R5P concentration

(A) Size-exclusion chromatography of wild type (WT, green trace) and ΔECTD pyruvate kinase (blue trace) with apparent molecular masses of approximately 239 and 191 kDa, respectively, corresponding to the theoretical masses of 258.0 (monomeric mass of 64.5 kDa) and 212.8 kDa (monomeric mass of 53.2 kDa) for homoterameric wild type and ΔECTD pyruvate kinase. The black trace represents the average partition coefficients and linear regression thereof of a protein standard containing thyroglobulin (669 kDa), ferritin (440 kDa), aldolase (158 kDa), conalbumin (75 kDa), ovalbumin (43 kDa), and RNase A (13.7 kDa). (B) Left: Schematics of pyruvate kinase activity assay using a coupled enzyme reaction. Pyruvate produced by pyruvate kinase is subsequently used by lactate dehydrogenase to oxidize NADH to NAD^+, leading to decreased

absorption at 340 nm by NADH. Pyk: pyruvate kinase; LDH: lactate dehydrogenase. LDH is added in excess to ensure not to be the rate limiting step. Right: The direct readout of pyruvate kinase enzyme activity assay with or without ATP. Absorbance at 340 nm is proportional to NADH concentration, and the slope of the curve is proportional to the pyruvate kinase activity. (C) ATP inhibition curve of wild type and ΔECTD pyruvate kinase. (D) Wild type and (E) ΔECTD pyruvate kinase activities in the presence of allosteric effectors. Reactions were performed with 20 nM Pyruvate kinase, 1.5 mM of PEP, 1 mM of ADP, 25 U/mL LDH, and 0.3 mM NADH. 5 mM ATP, 1 mM AMP, and 1 mM R5P were added as different effectors. F test was performed for each group, followed by Tukey's HSD test. p values of Tukey's HSD test are labeled in the figure if smaller than 0.05, p values larger than 0.05 are labeled as n.s. (not significant). (F) Wild type and (G) ΔECTD pyruvate kinase activities at different concentrations of the substrate PEP and activator R5P as indicated. The substrate ADP was provided at a concentration of 1 mM. All reactions also had 5 mM ATP inhibitor in the mix. Unit of the enzyme activity is molecules of pyruvate generated by one molecule of pyruvate kinase per second. Error bars represent standard error of the mean of triplicates. (H) Wild type and (I) ΔECTD pyruvate kinase activity data from (F) and (G) fitted to an adapted nonessential activation equation. The Hill coefficients for wild type and ΔECTD pyruvate kinase to PEP were 3.1 and 1.3, respectively.

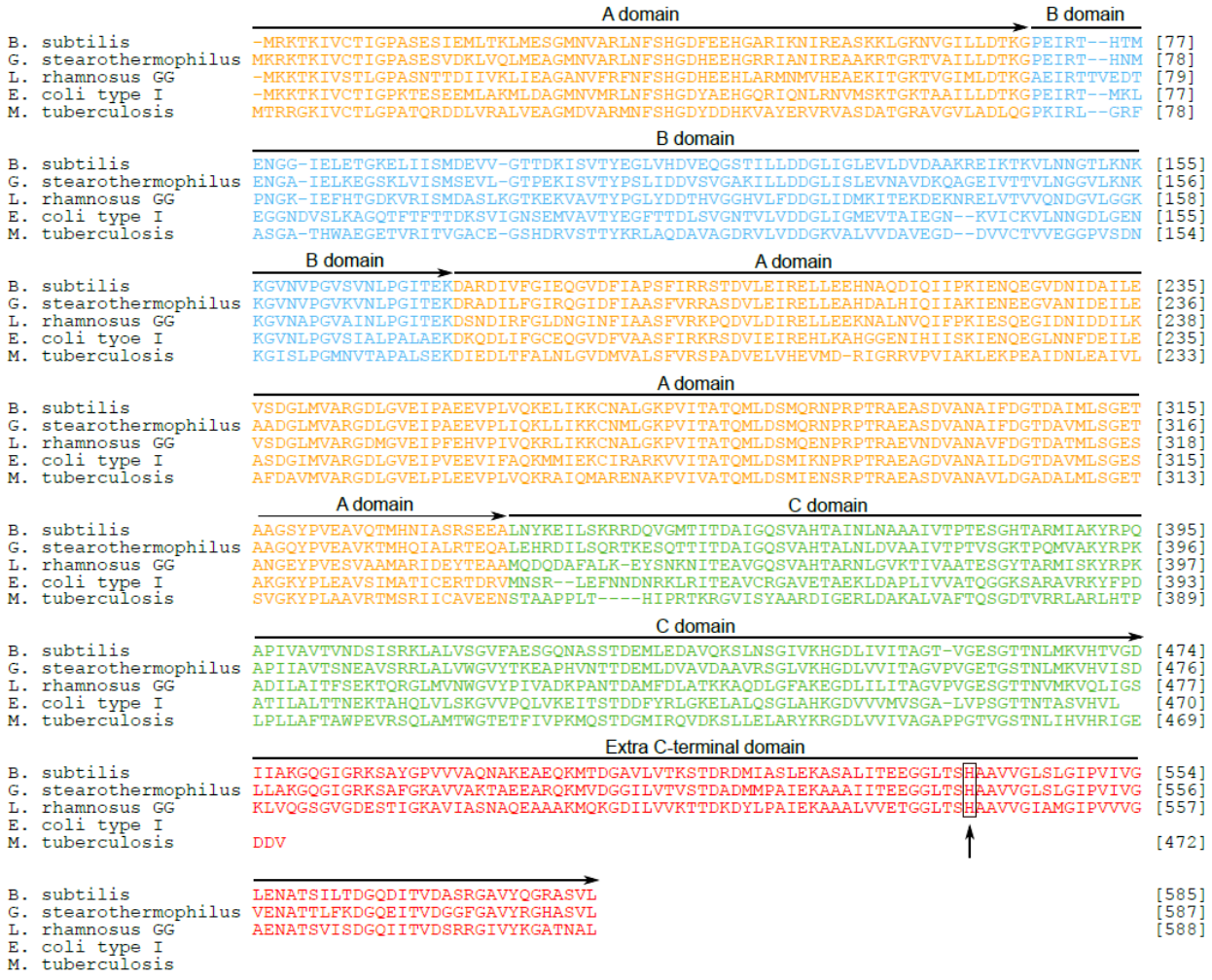

Supplementary Figure 1 Pyruvate kinases from some bacteria have an extra C-terminal domain

Alignment of pyruvate kinase sequences from different species. The active site is in a pocket between the A domain and B domain. The C domain is a regulatory domain with effector binding sites. The conserved active histidine in the ECTD is labeled by an arrow.

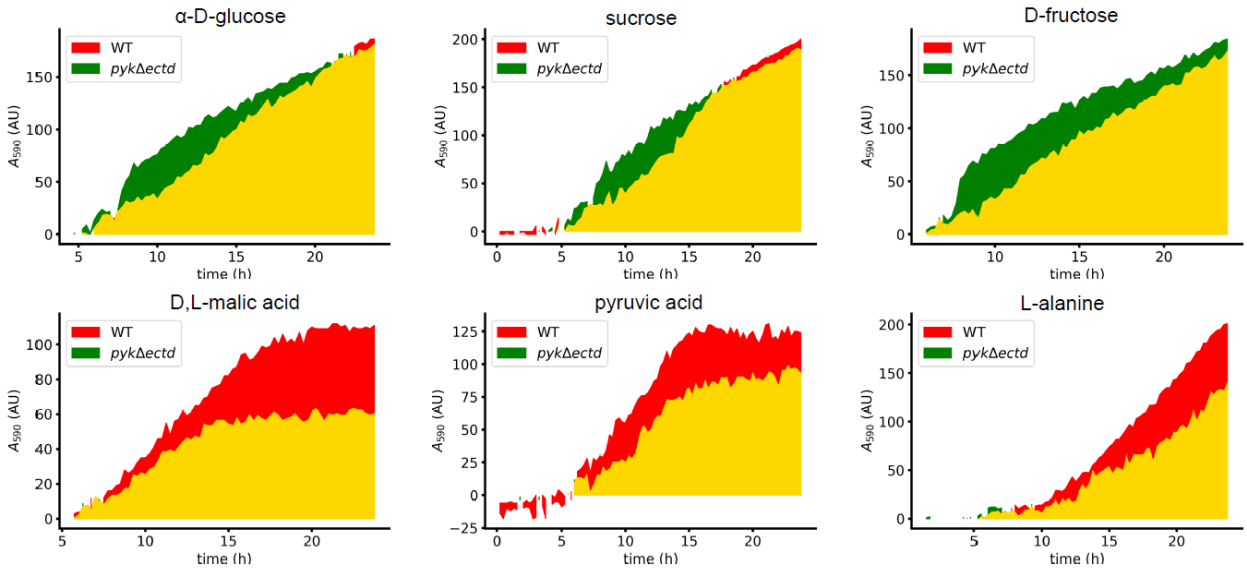

Supplementary Figure 2 Phenotypic screen for *pykΔectd* mutant

Examples of phenotype screening result. Cells were inoculated in media with the indicated carbon sources and the redox dye to measure cellular respiration as a reporter of growth. Area under wild type curve is colored red, area under *pykΔectd* curve is colored green, overlapping region is colored yellow.

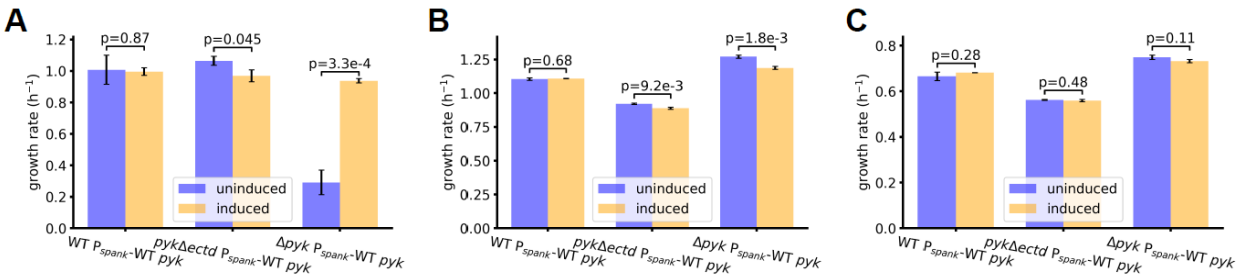

Supplementary Figure 3 Complementation tests of *pyk mutant* alleles

Growth rates of wild type *pyk*, the *pykΔectd* mutant, or the *Δpyk* mutant alleles complemented with wild type *pyk* growing in glycolytic (Glucose, A) or gluconeogenic (malate, B or pyruvate, C) media. Wild type *pyk* was provided ectopically at the *amyE* locus with an IPTG-inducible promoter.

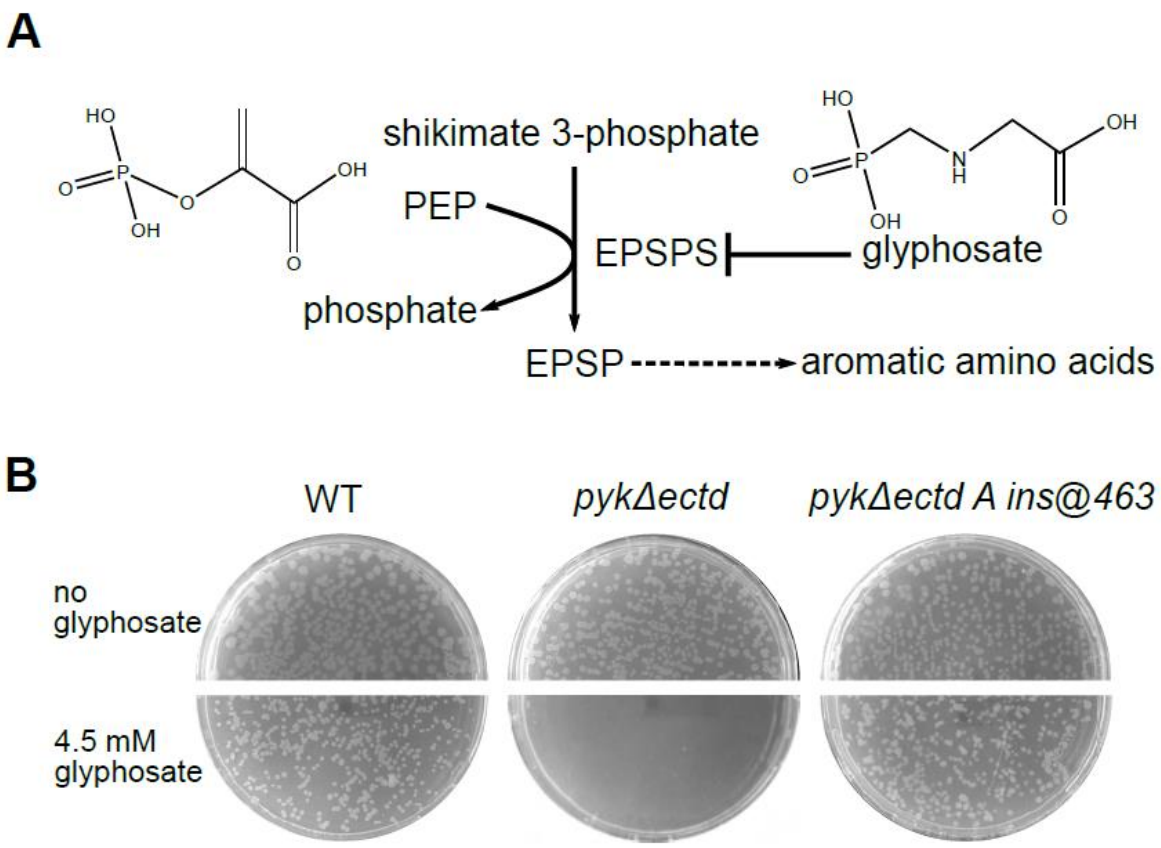

Supplementary Figure 4 Hypersensitivity of *pykΔectd* mutant to glyphosate can be suppressed by a loss-of-function mutation

(A) Glyphosate inhibits the shikimate pathway, which is required for the synthesis of aromatic amino acids by competing with PEP. (B) Plate images of wild type, *pykΔectd*, and glyphosate suppressor on malate minimal plates with or without glyphosate.

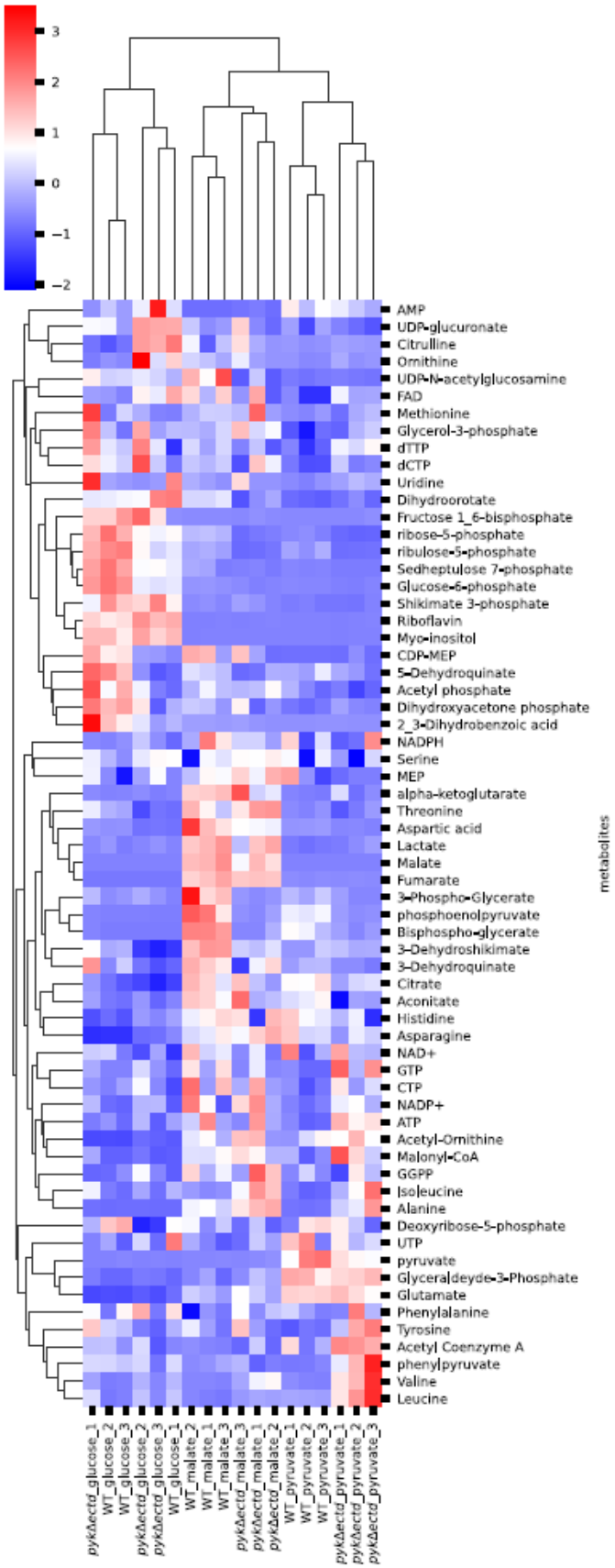
3
2
1
0
−1
−2
AMP
UDP-glucuronate
Citrulline
Ornithine
UDP-N-acetylglucosamine
FAD
Methionine
Glycerol-3-phosphate
dTTP
dCTP
Uridine
Dihydroorotate
Fructose 1_6-bisphosphate
ribose-5-phosphate
ribulose-5-phosphate
Sedheptulose 7-phosphate
Glucose-6-phosphate
Shikimate 3-phosphate
Riboflavin
Myo-inositol
CDP-MEP
5-Dehydroquinate
Acetyl phosphate
Dihydroxyacetone phosphate
2_3-Dihydrobenzoic acid
NADPH
Serine
MEP
alpha-ketoglutarate
Threonine
Aspartic acid
Lactate
Malate
Fumarate
3-Phospho-Glycerate
phosphoenolpyruvate
Bisphospho-glycerate
3-Dehydroshikimate
3-Dehydroquinate
Citrate
Aconitate
Histidine
Asparagine
NAD+
GTP
CTP
NADP+
ATP
Acetyl-Ornithine
Malonyl-CoA
GGPP
Isoleucine
Alanine
Deoxyribose-5-phosphate
UTP
pyruvate
Glyceraldeyde-3-Phosphate
Glutamate
Phenylalanine
Tyrosine
Acetyl Coenzyme A
phenylpyruvate
Valine
Leucine
metabolites
pykΔectd_glucose_1
WT_glucose_2
WT_glucose_3
pykΔectd_glucose_2
pykΔectd_glucose_3
WT_glucose_1
WT_malate_2
WT_malate_1
WT_malate_3
pykΔectd_malate_3
pykΔectd_malate_1
pykΔectd_malate_2
WT_pyruvate_1
WT_pyruvate_2
WT_pyruvate_3
pykΔectd_pyruvate_1
pykΔectd_pyruvate_2
pykΔectd_pyruvate_3

Supplementary Figure 5 Metabolome of wild type and *pykΔectd* mutant in glycolytic or gluconeogenic media

Heatmap of metabolites of wild type and *pykΔectd* cells grown in media with different carbon sources. Rows and columns are clustered with UPGMA (unweighted pair group method with arithmetic mean). Color represents Z scores for rows.

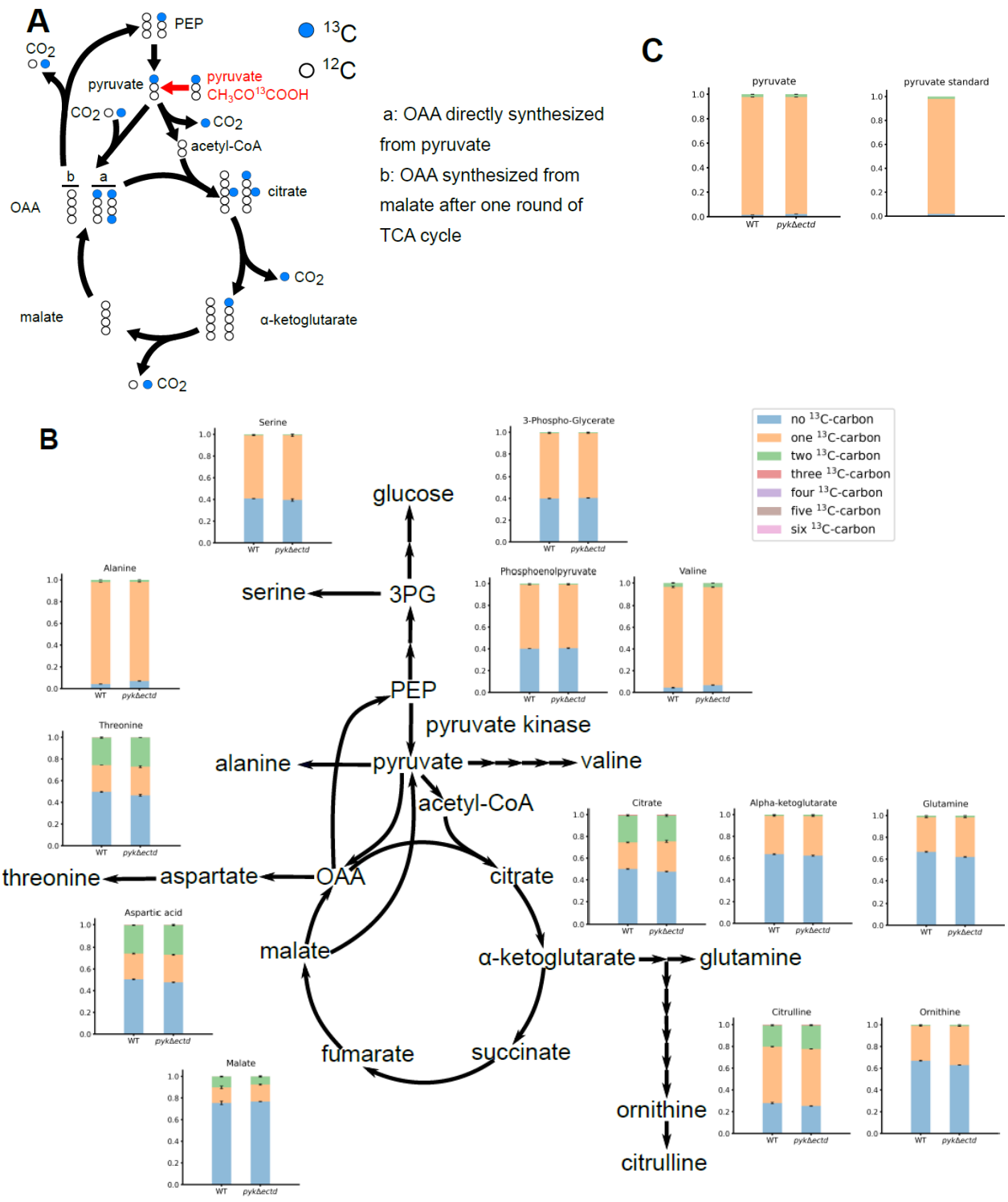

Supplementary Figure 6 Isotope composition of important metabolites in cells grown in media with [1-^{13}C] pyruvate

(A) Proposed labeling of PEP and TCA cycle intermediates with [1-^{13}C] pyruvate. In *B. subtilis*, PEP carboxykinase, which converts oxaloacetate (OAA) to PEP, is the only enzyme that regenerates PEP from TCA cycle intermediates. Therefore, when pyruvate is the sole carbon source, all PEP is produced from OAA. OAA can be synthesized from pyruvate directly via pyruvate carboxylase or from malate by malate dehydrogenase. When cells are grown on [1-^{13}C] pyruvate, OAA directly synthesized from pyruvate is [1-^{13}C] labeled. However, OAA synthesized from malate after one round of the TCA cycle is unlabeled. Therefore, only a fraction of OAA is expected to be labeled, as well as PEP since it is derived from OAA. (B) Wild type and *pykΔectd* cells were grown in media with [1-^{13}C] pyruvate as the sole carbon source; isotope composition of intracellular metabolites was analyzed by LC-MS. Isotope composition of some metabolites in gluconeogenesis and TCA cycle and of some amino acids is shown here. (C) Isotope composition of pyruvate in cells (left) and in the media (right).

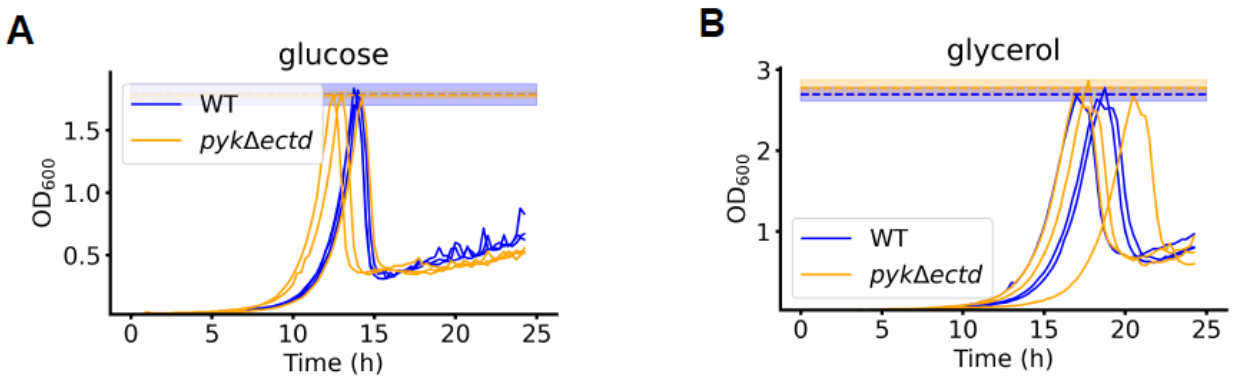

Supplementary Figure 7 Maximum OD of wild type or *pykΔectd* cells grown in media with different glycolytic sole carbon sources

Growth curves of wild type or *pykΔectd* cells in media with 2 g/L (A) glucose or (B) glycerol. Dashed lines represent the average maximum ODs for each condition, and the colored regions represent the 95% confidence interval.

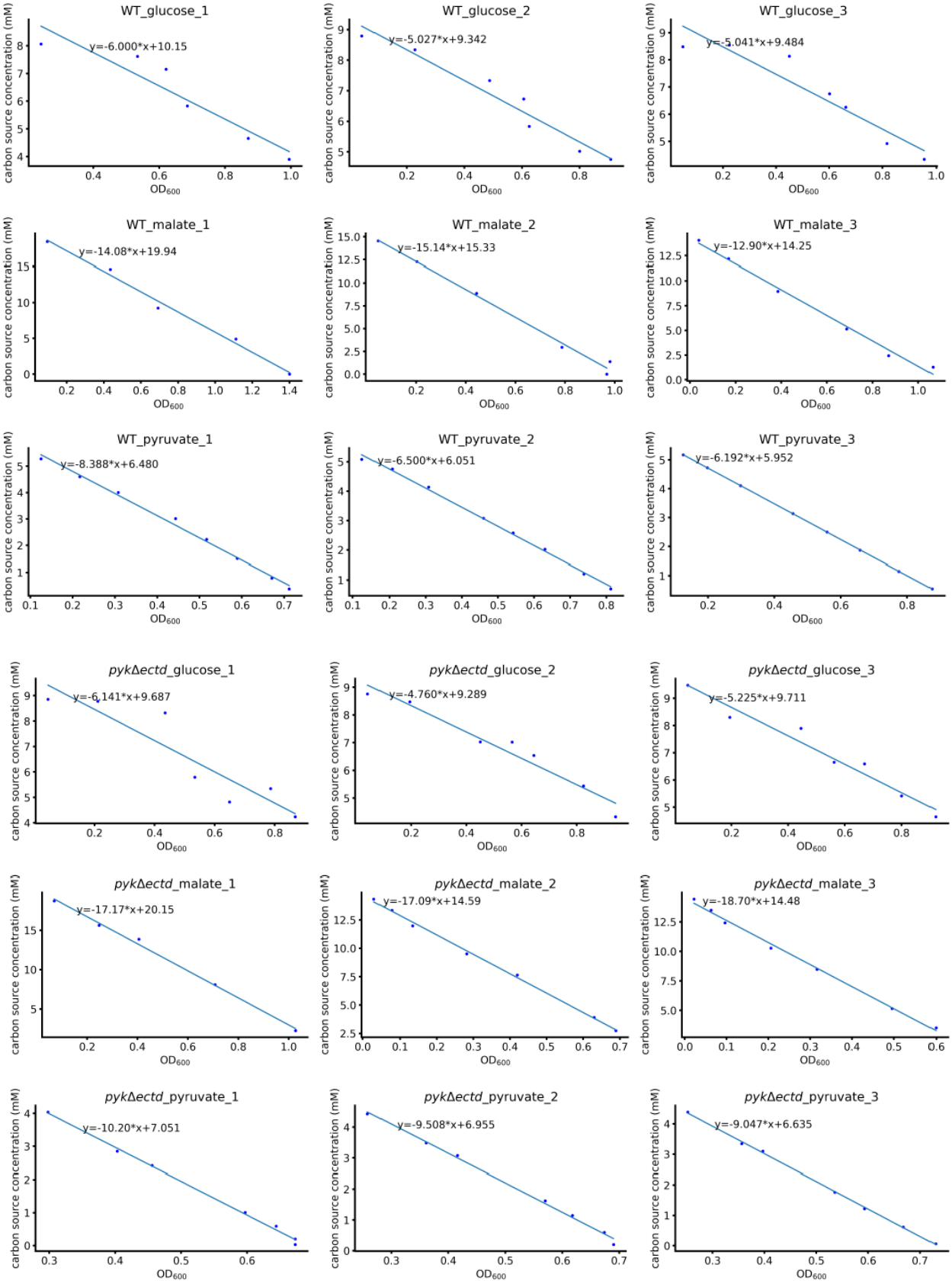
WT_glucose_1
y=-6.000*x+10.15
WT_glucose_2
y=-5.027*x+9.342
WT_glucose_3
y=-5.041*x+9.484
WT_malate_1
y=-14.08*x+19.94
WT_malate_2
y=-15.14*x+15.33
WT_malate_3
y=-12.90*x+14.25
WT_pyruvate_1
y=-8.388*x+6.480
WT_pyruvate_2
y=-6.500*x+6.051
WT_pyruvate_3
y=-6.192*x+5.952
pykΔectd_glucose_1
y=-6.141*x+9.687
pykΔectd_glucose_2
y=-4.760*x+9.289
pykΔectd_glucose_3
y=-5.225*x+9.711
pykΔectd_malate_1
y=-17.17*x+20.15
pykΔectd_malate_2
y=-17.09*x+14.59
pykΔectd_malate_3
y=-18.70*x+14.48
pykΔectd_pyruvate_1
y=-10.20*x+7.051
pykΔectd_pyruvate_2
y=-9.508*x+6.955
pykΔectd_pyruvate_3
y=-9.047*x+6.635
carbon source concentration (mM)
OD600

Supplementary Figure 8 Gluconeogenic carbon use efficiency of *pykΔectd* mutant is lower than the wild type strain

Carbon sources left in media plotted versus OD of cells. Slopes are calculated by linear regression with the method of least squares and represent carbon use efficiency.

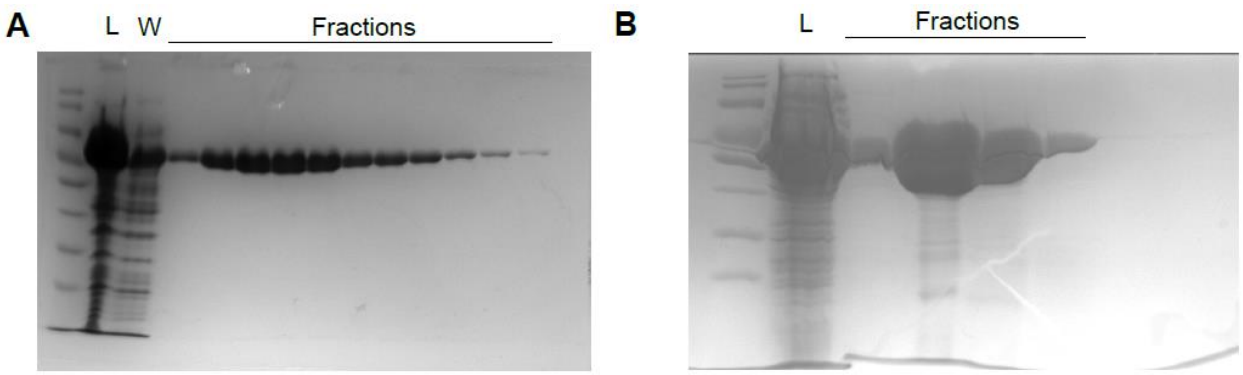

Supplementary Figure 9 Purification of *B. subtilis* pyruvate kinases

Coomassie brilliant blue stained SDS-PAGE gel of 6x His tagged *B. subtilis* (A) wild type pyruvate kinase and (B) ΔECTD pyruvate kinase purified with Ni-NTA column. L: lysate; W: wash.

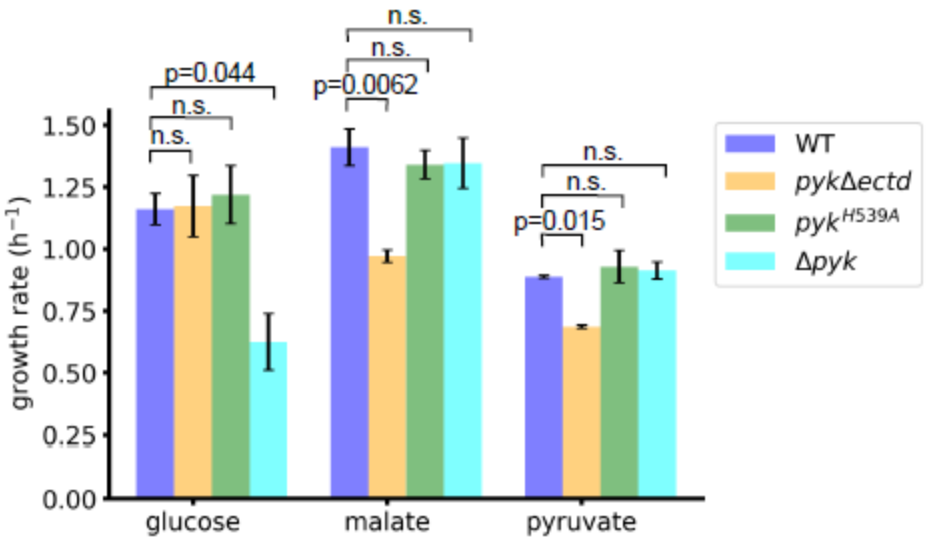

Supplementary Figure 10 Conserved histidine on pyruvate kinase ECTD is not responsible for the inhibition of pyruvate kinase activity during gluconeogenic growth

Growth rate of wild type, *pykΔectd*, *pyk*^{H539A} and *Δpyk* cells in media with different sole carbon sources, data of wild type, *pykΔectd* and *Δpyk* cells are the same as Figure 1C and 1D. F test was performed for each group, followed by Tukey's HSD test. p value of F test for glucose group: 1.7e-2, for malate group: 3.3e-3, for pyruvate group: 1.4e-3. p values of Tukey's HSD test are labeled in the figure if smaller than 0.05, p values larger than 0.05 are labeled as n.s. (not significant).

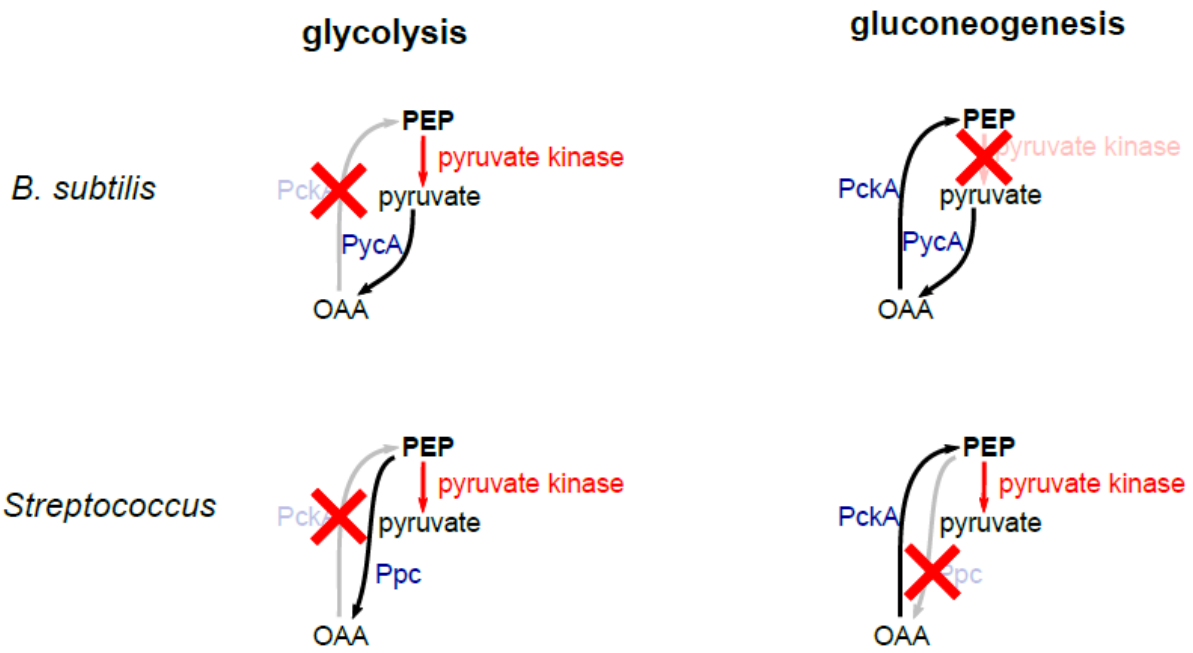

Supplementary Figure 11. Comparison of the futile cycle model between *B. subtilis* and *Streptococcus* species

Ppc instead of PycA acts as the anaplerotic enzyme in *Streptococcus* species. This excludes pyruvate kinase from the potential futile cycle. PycA: pyruvate carboxylase; PckA: PEP carboxykinase; Ppc: PEP carboxylase.

Chapter 3: Loss of function mutations of pyruvate kinase suppress guanosine toxicity

Kuanqing Liu[1,*], **Fukang She**[1,*], Brent W Anderson[1], Tippapha Pisithkul[1], Tyler McCue[1], William Mulhern[1], Daniel Amador-Noguez[1], Jue D. Wang[1]

[1]Department of Bacteriology, University of Wisconsin-Madison, Madison, Wisconsin, USA

*These authors contribute equally.

Author contributions

K.L., F.S., B.W.A., J.D.W. and D.A.N designed the research. K.L., F.S., T.P., T.M. and W.M. performed experiments. K.L., F.S., B.W.A, D.A.N and J.D.W analyzed data. K.L. and F.S. wrote the paper. F.S. and J.D.W edited the paper.

This chapter will be submitted to Journal of Bacteriology.

Abstract

Stress response is vital for bacterial survival and adaptation in diverse environments. Guanosine pentaphosphate and guanosine tetraphosphate [(p)ppGpp], two nucleotide signaling molecules involved in stress response in virtually all bacteria, have been found to regulate purine nucleotide synthesis and resource partition between macromolecule synthesis and stress response. In this study, we investigated the impact of (p)ppGpp deficiency in a *Bacillus subtilis* strain with dysregulated GTP levels, which resulted in diminished cell vitality when exposed to extracellular guanosine. We found that guanylate kinase (GMK) and hypoxanthine phosphoribosyltransferase (HPRT) mutations suppressed guanosine toxicity by decreasing the GTP level. Intriguingly, we also discovered that loss-of-function mutations in the central carbon metabolism enzyme pyruvate kinase were effective in mitigating guanosine toxicity. Combining *in vitro* enzyme kinetics and *in vivo* metabolism experiments, we identified two potential mechanisms: Firstly, the loss of pyruvate kinase enzyme activity decreased the GTP synthesis by pyruvate kinase in the absence of (p)ppGpp, and secondly, pyruvate kinase mutations rescued the depletion of glycolysis intermediates caused by the absence of (p)ppGpp. Altogether, our findings demonstrate the involvement of pyruvate kinase in nucleotide synthesis and resource allocation in carbon metabolism.

Introduction

Purine nucleotides are small molecules that play crucial roles in cell physiology, as they provide the building blocks for nucleic acid synthesis, carry cellular energy for metabolism, and participate in signaling and enzymatic reactions. In most organisms, they are synthesized by the *de novo* and salvage pathways. The former is a multistep process that begins with PRPP (5-phosphoribosyl-α-1-pyrophosphate) and requires heavy investment of cellular resources, whereas the latter represents an economic route to synthesize purine nucleotides by simply recycling purine nucleosides and bases.

However, it is reported that these two pathways do not operate freely and are in fact subject to stringent regulations that occur at both the gene and protein level[1–3]. The regulation of these two pathways relies on two highly phosphorylated nucleotides, guanosine tetra- and pentaphosphate, collectively named (p)ppGpp. (p)ppGpp is produced during stress by RelA, SasA or SasB by pyrophosphorylating GTP or GDP with ATP in *B. subtilis*. Once produced, (p)ppGpp directly inhibits the *de novo* pathway as an anti-inducer of PurR, the repressor of Pur operon, which encodes the *de novo* synthesis enzymes. (p)ppGpp also directly inhibits the salvage pathway by inhibiting salvage pathway enzymes hypoxanthine phosphoribosyltransferase (HPRT) and guanylate kinase (GMK). These regulations are crucial for cells to maintain purine nucleotide homeostasis. For example, if guanosine is added from the environment to *B. subtilis* that lost all three (p)ppGpp synthetases, which is denoted (p)ppGpp^0 strain, then GTP levels will raise rapidly, with accompanying cell death[4].

What is the source of cell death due to elevated GTP (death-by-GTP)? In order to understand the critical role of (p)ppGpp in GTP homeostasis, we conducted a genetic selection to identify suppressors of guanosine toxicity and employed liquid chromatography coupled with mass spectrometry (LC-MS) to characterize the effects of (p)ppGpp deficiency and the suppressor mutations. Our findings demonstrate that, apart from the genes involved in GTP

synthesis pathways (*gmk* and *hprT*), loss-of-function mutations in the *pyk* gene, encoding pyruvate kinase in the glycolysis pathway, can effectively alleviate guanosine toxicity. These mutations resulted in a reduction in GTP synthesis from GDP and compensated for the depletion of glycolytic intermediates caused by hyperactive nucleotide synthesis. These observations highlight the crucial role of pyruvate kinase in nucleotide metabolism and carbon resource allocation, as well as the regulatory function of (p)ppGpp in the allocation of resources between nucleotides and other biosynthetic pathways.

Results

Guanosine treatment drastically increased intracellular GMP, GDP, and GTP in (p)ppGpp^0 cells

In *B. subtilis*, (p)ppGpp inhibits HPRT and GMK of the GTP biosynthesis pathways to maintain guanine nucleotide homeostasis (Figure 1A)[4,5]. Loss of this regulation, as observed in the (p)ppGpp^0 cells, leads to loss of viability when guanosine is added to the media[4] (Figure 1B), which *B. subtilis* can normally salvage to produce guanine nucleotides. It is unclear how this toxicity occurs, but early work using thin layer chromatography (TLC) linked it to high GTP levels[4]. To gain further insight into guanosine toxicity, we performed liquid chromatography coupled to mass spectrometry (LC-MS) to track guanosine metabolism. Upon guanosine treatment, both WT and (p)ppGpp^0 cells rapidly accumulated guanosine and guanine, but GMP, GDP, and GTP remained low in WT because of the inhibition of (p)ppGpp on HPRT and GMK. In contrast, (p)ppGpp^0 cells rapidly accumulate GMP, GDP and GTP, as well as guanosine and guanine, to an abnormally high level (Figure 1C). This observation was consistent with the notion that (p)ppGpp maintains homeostasis of the guanine nucleotide pool via a negative feedback loop (Figure 1A).

Genetic selections for spontaneous suppressor of (p)ppGpp0 guanosine toxicity

The surge of GMP, GDP, and GTP in (p)ppGpp^0 (Figure 1C) alluded to the possibility that guanine nucleotide surplus might be detrimental, but which nucleotide(s) was the culprit remained elusive. To tackle this question, we carried out an unbiased genetic selection by taking advantage of the fact that (p)ppGpp^0 cells cannot form colonies with exogenous guanosine[4]. We inoculated (p)ppGpp^0 cells in separate culture tubes, grew the culture to stationary phase to allow independent spontaneous generation of suppressors, and then plated each culture onto what agar media with 0.1 mM guanosine. (p)pppGpp^0 cells are not able to form colonies.

However, spontaneously occurring suppressors were able to form colonies at a low frequency. One colony from each plate was subsequently collected, analyzed for their GTP levels using TLC and sequenced for identification of the suppressor alleles (Table 1, Figure 2).

Loss-of-function mutations in *hprt* and *gmk* of the GTP biosynthesis pathway suppressed guanosine toxicity

Because guanosine treatment of (p)ppGpp^0 cells results in high level of GTP that is associated with loss of viability, we anticipated the suppressors to bear loss-of-function mutations in genes of the GTP biosynthesis pathways. We therefore performed targeted Sanger sequencing in genes *hprt* and *gmk*, which encoded HPRT and GMK, respectively. We identified insertions and deletions, as well as point mutations that either change a single amino acid or the putative Shine-Dalgarno sequence, in *hprT* (Figure 2A). For the *gmk* suppressors, we had identified only missense mutations (Figure 2C), this is because *gmk* is an essential gene. No supressors were identified in *guaB, codY*, unlike our previous screen for minimal media without amino acid. This is expected, because these genes are exclusively in the de novo synthesis pathway. Nonetheless, the discovery of *hprt* and *gmk* suppressors provided genetic evidence to further support the proposition that (p)ppGpp inhibited HPRT and GMK to maintain guanine nucleotide homeostasis. Importantly, the identification of *gmk* suppressors implied that high GMP was unlikely to be the culprit for cell death, leaving GDP or GTP solely associated with unviability.

Loss of function mutations in *pyk* rescued guanosine toxicity

Interestingly, in addition to low GTP suppressors, we also isolated eight suppressors, whose GTP levels rose more than 4-fold upon guanosine treatment (Figure 2E and 2F). By combining whole genome sequencing (WGS) and targeted Sanger sequencing, we found that

mutations were mapped exclusively to the *pyk* gene that encodes pyruvate kinase (PK). PK catalyzed the conversion of phosphoenolpyruvate to pyruvate using NDP as the phosphate recipient and functioned as a key enzyme in glycolysis. To understand how *pyk* mutations suppressed guanosine toxicity, we focused on the *pyk*^{G318E} mutant since it was the first *pyk* mutant isolated and its genome had been completely sequenced. *In vitro* enzymatic assay using recombinant PK revealed that the G318E mutation severely impaired its enzyme activity (Figure 3A), suggesting that loss-of-function mutation in *pyk* rescued guanosine toxicity. We further tested that a clean deletion of *pyk* in (p)ppGpp^0 cells rescued guanosine toxicity (Figure 3B), confirmed that loss-of-function mutation in *pyk* could rescue guanosine toxicity.

Pyruvate kinase is mainly a GTP producer under physiological conditions

Next, we examined the (p)ppGpp^0 *pyk* suppressors, aiming to understand how it may rescue the guanosine toxicity due to lack of (p)ppGpp. First, we noticed that although the GTP levels in *pyk* mutants were higher than WT after guanosine treatment, it was still lower than those in (p)ppGpp^0 cells (Figure 2F). To understand how *pyk* mutations lead to lowered GTP levels, we compared metabolomic data of (p)ppGpp^0 cells and (p)ppGpp^0 *pyk*^{G318E} cells. We noticed that, comparing to WT cells, GTP was accumulated to 7-fold in (p)ppGpp^0 cells and to 4-fold in (p)ppGpp^0 *pyk*^{G318E} cells; Instead, GDP was accumulated to 6-fold in (p)ppGpp^0 cells and 19-fold in (p)ppGpp^0 *pyk*^{G318E} cells (Figure 3C, Supplementary Figure 1). The flow from GDP to GTP was blocked by loss of function of *pyk*. Although pyruvate kinase has been mostly described in textbook[3] as using ADP and PEP as substrates and ATP and pyruvate as product, it has been long been known as a promiscuous enzyme using different NDPs as the substrate. Our *in vivo* result strongly implicates the role of pyruvate kinase in making GTP from GDP.which strongly implied the role of pyruvate kinase in making GTP from GDP. This also indicated that GDP was unlikely to be the culprit for cell death, it agreed with the conclusion that guanosine toxicity was associated with GTP level[4].

Pyruvate kinase is one of the enzymes catalyzing substrate-level phosphorylation, so we hypothesized that pyruvate kinase could efficiently synthesize GTP directly from GDP in *B. subtilis*. We expressed and purified *B. subtilis* pyruvate kinase and tested the substrate specificity *in vitro*. Consistent with previous reports, *B. subtilis* pyruvate kinase was capable of using both ADP and GDP as phosphate recipient, with $S_{0.5}$ at 2.53 mM and 0.48 mM respectively (Figure 4A, 4B). *B. subtilis* pyruvate kinase was capable to use CDP and UDP as substrates as well (Supplementary Figure 2). Pyruvate kinases were reported to be positively cooperative with respect to PEP, we shown that *B. subtilis* pyruvate kinase was also weakly positive cooperative with respect to ADP and GDP as well (Hill coefficient 1.20 and 1.44 respectively). We also noticed that AMP, as the activator of pyruvate kinase, could change the sigmoidal curve to hyperbolic curve with K_m at 1.12 mM and 0.036 mM respectively, indicating that AMP could help the binding of ADP or GDP.

Given the lower K_m of GDP, we further tested whether pyruvate kinase will use GDP as phosphate recipient better than ADP. We used strong anion exchange chromatography to separate and quantify GTP and ATP in the reaction (Supplementary Figure 3). Surprisingly, although pyruvate kinase used ADP faster than GDP individually, GTP was dominant in the products when both GDP and ADP were present and close to physiological concentration (Figure 4C and 4D). Given ADP and GDP are both available *in vivo*, pyruvate kinase is likely to mainly produce GTP as the product of substrate level phosphorylation.

Loss-of-function mutations of pyruvate kinase rescues the depletion of glycolysis intermediates

Nucleotides synthesis takes precursors from central carbon metabolism as well as nucleobases (Figure 5A). In wild type cells, the pools of guanine nucleotides and glycolysis intermediates remained stable following the addition of guanosine (Figure 5B). the guanine nucleotides pool exhibited a significant increase, whereas the level of glycolysis intermediates

decreased after guanosine treatment (Figure 5B), which is possibly the result of fulfilling the demand of nucleotides synthesis. Intriguingly, in (p)ppGpp^0 *pyk*$^-$ cells, although glycolysis intermediates level was still decreasing upon the guanosine treatment, the levels of glycolysis intermediates were higher than (p)ppGpp^0 cell but closer to wild type cells (Figure 5B). This discrepancy was attributed to the accumulation of PEP caused by the loss of pyruvate kinase activity. To test whether loss-of-function of pyruvate kinase mitigates guanosine toxicity via compensating glycolysis intermediates, we grew wild type, (p)ppGpp^0 and (p)ppGpp^0 *pyk*$^-$ cells in glucose media or pyruvate media with or without guanosine. We found that wild type and (p)ppGpp^0 cells responded similarly in both glucose media and pyruvate media. However, (p)ppGpp^0 *pyk*$^-$ cells displayed increased sensitivity to extracellular guanosine in pyruvate media, indicating that glucose is required for suppressing guanosine toxicity by the *pyk* mutation. This supports the idea that loss-of-function mutation of pyruvate kinase compensates for the depletion of glycolysis intermediates resulting from the absence of (p)ppGpp regulation.

Discussion

Pyruvate kinase catalyzes the last step in glycolysis, generating energy from substrate level phosphorylation. Bacterial pyruvate kinase has been observed to use a broad range of nucleoside diphosphate as phosphoryl group recipient, with ADP typically being the most favorable choice[6]. However, we found that GDP is the preferred phosphoryl group recipient for *Bacillus subtilis* pyruvate kinase, suggesting that pyruvate kinase likely plays a significant role in GTP production *in vivo.*

Loss-of-function mutation of pyruvate kinase rescues guanosine toxicity potentially via decreasing GTP production from GDP, which raises a question that why no *ndk* suppressor was found. One possibility is that as well as substrate level phosphorylation, pyruvate kinase also provides material for the TCA cycle and oxidative phosphorylation. Loss of function of pyruvate

kinase leads to less oxidative phosphorylation, which causes decrease of adenyl energy charge (Supplementary Figure 4). NDK activity is presumably inhibited by low energy charge[7], this contributes to blocking GTP synthesis from GDP as well. *pyk* mutant has combined effect of loss of direct GTP synthesis from PK and weakened NDK activity, as well as compensation of glycolysis intermediates, this might explain why *ndk* did not appear in suppressor selection.

(p)ppGpp tightly regulates purine nucleotides synthesis, balancing the resource allocation between nucleotides and carbon metabolism. In wild type cells, (p)ppGpp prevents overactive nucleotide synthesis via inhibiting the expression of purine synthesis enzymes or direct inhibition[8] of the activity of purine synthesis enzymes such as HPRT and GMK[5,9]. In the absence of (p)ppGpp regulation, (p)ppGpp^0 cells produce GTP overwhelmingly, which drains the carbon from the central carbon metabolism. The reaction catalyzed by pyruvate kinase lies at the junction between the glycolysis and the TCA cycle, it plays an important role in allocating the carbon resources to different pathways. Low pyruvate kinase activity leads to the accumulation of glycolysis intermediates, which potentially compensates for the depletion of precursors caused by dysregulated nucleotide synthesis in (p)ppGpp^0 cells.

We showed that a classical central carbon metabolism enzyme pyruvate kinase is involved in the nucleotides synthesis directly, and together with (p)ppGpp, regulates the resource allocation in nucleotide metabolism and carbon metabolism. The network nature of metabolism allows complicated regulation to deal with fluctuating environmental conditions, maintaining the homeostasis of the cell.

Table 1. List of suppressors that rescue guanosine toxicity of (p)ppGpp^0 mutants

Strain Name	Genotype	Reference

JDW94	*trpC2, metB10, xin-1,* SPβ	Yasbin et al.[10]
JDW755	JDW94 *ΔyjbM ywaC*::*kan relA*::*mls*	Kriel et al.[4]
JDW1854	JDW755 *hprt -16 G>A*	This work
JDW1850	JDW755 *hprt* +14 A insertion	This work
JDW1839	JDW755 *hprt* ^{L37S}	This work
JDW1853	JDW755*hprt* +164 to +207 deletion	This work
JDW1848	JDW755 *hprt*^{D103G}	This work
JDW1858	JDW755 *hprt*^{G105D}	This work
JDW1852	JDW755 *hprt*^{T107I}	This work
JDW1856	JDW755 *hprt*^{T107I}	This work
JDW1849	JDW755 *hprt*^{R165C}	This work
JDW1851	JDW755 *hprt*^{R165C}	This work
JDW1834	JDW755 *hprt* +333 TC insertion	This work
JDW1835	JDW755 *gmk*^{R4R}	This work
JDW1837	JDW755 *gmk*^{Y54F}	This work
JDW1845	JDW755 *gmk*^{G83S}	This work
JDW1841	JDW755 *gmk*^{G83S}	This work
JDW1833	JDW755 *gmk*^{D98G}	This work
JDW1826	JDW755 *gmk*^{N148K}	This work
JDW1836	JDW755 *gmk*^{Y163D}	This work
JDW1847	JDW755 *pyk*^{H37R}	This work
JDW1843	JDW755 *pyk*^{D66N}	This work
JDW1838	JDW755 *pyk*^{D125A}	This work
JDW1840	JDW755 *pyk*^{A190V}	This work
JDW1857	JDW755 *pyk*^{G318E}	This work

JDW1832	JDW755 *pyk* +423 Nonsense	This work
JDW1846	JDW755 *pyk* +468 A insertion	This work
JDW1830	JDW755 *pyk* +783 A insertion	This work

Materials and Methods

Strains and growth conditions

All *Bacillus subtilis* strains were derived from YB866 or NCIB3610 (Table 1). Growth media was either S7 or Spizizen salt based supplemented with 0.5% (w/v) casamino acids (CAS), with 40 µg ml^{-1} tryptophan and methionine[4] or not. Guanosine was suspended in sterile Milli-Q water and used at a final concentration of 0.1 mM in agar plates and 1 mM in liquid broth, respectively.

Suppressor selection and verification

Single colonies of (p)ppGpp^0 were grown independently in S7 + CAS to saturation. An aliquot of 100 µl culture was plated directly onto Spiz + CAS with 0.1 mM guanosine. Only one suppressor was selected from each plate and the suppressor was verified by its ability to survive 0.1 mM guanosine on agar plates.

Suppressor mutation identification

Sanger sequencing targeting genes in the GTP biosynthesis pathway was performed for the low GTP group (≤ 2 fold change of GTP levels relative to untreated). Mutations in the high GTP group (>2 fold change of GTP levels relative to untreated) were identified by whole genome sequencing and targeted Sanger sequencing as described previously[4,11].

Thin layer chromatography (TLC)

TLC was performed exactly as described[12]. Briefly, *B. subtilis* cells were grown in low phosphate (0.5 mM) S7 with 0.5% (w/v) casamino acids and labeled with 50 μCi ml^{-1} ^{32}P orthophosphate (900 mCi $mmol^{-1}$; Perkin-Elmer) for 2 – 3 generations before sampling. Nucleotides were extracted by incubating 100 μl culture with 20 μl 2 M formic acid on ice for at least 20 minutes. Samples were spotted onto a cellulose PEI plate and separated in 1.5 M KH_2PO_4 (pH 3.4). The TLC plates were exposed to a storage phosphor screen. Nucleotides were detected by scanning with a Typhoon scanner (GE) and quantified using the ImageQuant software (Molecular Dynamics).

LC-MS metabolomics

Cells were grown in modified S7 medium (5 mM MOPS) until OD_{600} reached 0.3, and guanosine was added to a final concentration of 1 mM. Before and after guanosine treatment, 5 ml samples were taken for metabolite extraction and analyzed by LC-MS as described previously[5].

Expression, purification, and enzymatic assay of pyruvate kinase

The coding sequence of *B. subtilis pyk* was PCR amplified and cloned into the pLICtrPC-HA vector by ligation independent cloning[13]. The recombinant plasmid was verified by Sanger sequencing and transformed into *Escherichia coli* BL21 (DE3) cells (Agilent Technologies). Cultures were grown at 37°C in Lysogeny Broth (LB) with 100 μg ml^{-1} carbenicillin to an OD_{600} ~ 0.5 and induced with 1 mM IPTG for 3 hours before harvest. Cell were disrupted in 500 mM NaCl, 20 mM NaH_2PO_4, and 10 mM imidazole by passing through a French press twice. Cell debris was cleared by centrifugation and the supernatant was loaded onto a HisTrap FF column (GE Healthcare) using an ÄKTA FPLC (GE Healthcare). The N terminal His-tagged pyruvate kinase was eluted using a linear gradient of imidazole in 500 mM NaCl and 20 mM NaH_2PO_4 and dialyzed in 40 mM Tris-HCl (pH 7.5), 50 mM NaCl, 1 mM EDTA, and 1 mM DTT. His-tag

was cleaved by TEV protease (1 mg TEV protease for 1L culture), untagged pyruvate kinase was collected by flowing through HisTrap FF column. Purified pyruvate kinase was analyzed by SDS-PAGE and quantified by Bradford assay (Bio-Rad).

Activity of pyruvate kinase was assayed at 25 °C in a 100 µl mix containing 100 mM Tris-HCl (pH 7.5), 100 mM KCl, 10 mM $MgCl_2$, 1.5 mM phospho(enol)pyruvate (PEP), 150 µM NADH, and 2U L-lactic dehydrogenase (from bovine muscle, Sigma-Aldrich), various concentration of ADP or GDP, and 20 nM pyruvate kinase. Reactions were monitored by measuring decrease of A_{340} in a Shimadzu UV-2401PC spectrophotometer for up to 5 minutes.

ADP/GDP competition assay

Reaction was in a 400 µl mix containing 100 mM Tris-HCl (pH=7.5), 100 mM KCl, 10 mM $MgCl_2$, 200 µM PEP, 500 µM ADP, 200 µM of GDP, 100 µM AMP, 20 nM pyruvate kinase. 350 µl mix was added to 14 µl 0.5 M EDTA at 1 min, 2 min, 3 min, 5 min and 10 min to stop reaction. 364 µl mix was diluted into 5 ml by ddH_2O, and then loaded onto HiTrap QFF 1 ml column (GE Healthcare) using an ÄKTA FPLC (GE Healthcare). GTP and ATP were eluted by a gradient of buffer A (25 mM citric acid, pH=3.5) and buffer B (25 mM citric acid, pH=3.5, 500 mM NaCl). Sample was injected with 5 ml buffer A, following by a wash with 5 column volume (CV) of buffer A. Elution was done by 5 CV linear gradient 0% buffer B to 12% buffer B, 10 CV 12% buffer B, 15 CV linear gradient 12% buffer B to 60% buffer B. Absorbance at 254 nm was recorded to detect nucleotides. AMP and ADP were eluted before 12% buffer B, GDP was eluted at 12% buffer B, ATP and GTP were eluted between 12% buffer B and 60% buffer B. The amount of ATP and GTP were quantified by a standard run with known concentration of ATP and GTP.

References

1. Rolfes, R. J. Regulation of purine nucleotide biosynthesis: in yeast and beyond. *Biochem. Soc. Trans.* **34**, 786–790 (2006).

2. Mandal, M., Boese, B., Barrick, J. E., Winkler, W. C. & Breaker, R. R. Riboswitches control fundamental biochemical pathways in Bacillus subtilis and other bacteria. *Cell* **113**, 577–586 (2003).

3. Nelson 1942-, D. L. (David L. *Lehninger principles of biochemistry*. (Fourth edition. New York : W.H. Freeman, 2005., 2005).

4. Kriel, A. *et al.* Direct regulation of GTP homeostasis by (p)ppGpp: a critical component of viability and stress resistance. *Mol. Cell* **48**, 231–241 (2012).

5. Liu, K. *et al.* Molecular mechanism and evolution of guanylate kinase regulation by (p)ppGpp. *Mol. Cell* **57**, 735–749 (2015).

6. Barzu, O. *et al.* Nucleotide specificity of pyruvate kinase and phosphoenolpyruvate carboxykinase. *Biochim. Biophys. Acta* **452**, 406–412 (1976).

7. Thompson, F. M. & Atkinson, D. E. Response of nucleoside diphosphate kinase to the adenylate energy charge. *Biochem. Biophys. Res. Commun.* **45**, 1581–1585 (1971).

8. Anderson, B. W. *et al.* The nucleotide messenger (p)ppGpp is an anti-inducer of the purine synthesis transcription regulator PurR in Bacillus. *Nucleic Acids Res.* **50**, 847–866 (2022).

9. Anderson, B. W. *et al.* Evolution of (p)ppGpp-HPRT regulation through diversification of an allosteric oligomeric interaction. *Elife* **8**, (2019).

10. Yasbin, R. E., Fields, P. I. & Andersen, B. J. Properties of Bacillus subtilis 168 derivatives freed of their natural prophages. *Gene* **12**, 155–159 (1980).

11. Srivatsan, A. *et al.* High-precision, whole-genome sequencing of laboratory strains facilitates genetic studies. *PLoS Genet.* **4**, e1000139 (2008).

12. Bittner, A. N., Kriel, A. & Wang, J. D. Lowering GTP level increases survival of amino acid starvation but slows growth rate for Bacillus subtilis cells lacking (p)ppGpp. *J. Bacteriol.* **196**, 2067–2076 (2014).

13. Stols, L. *et al.* A new vector for high-throughput, ligation-independent cloning encoding a tobacco etch virus protease cleavage site. *Protein Expr. Purif.* **25**, 8–15 (2002).

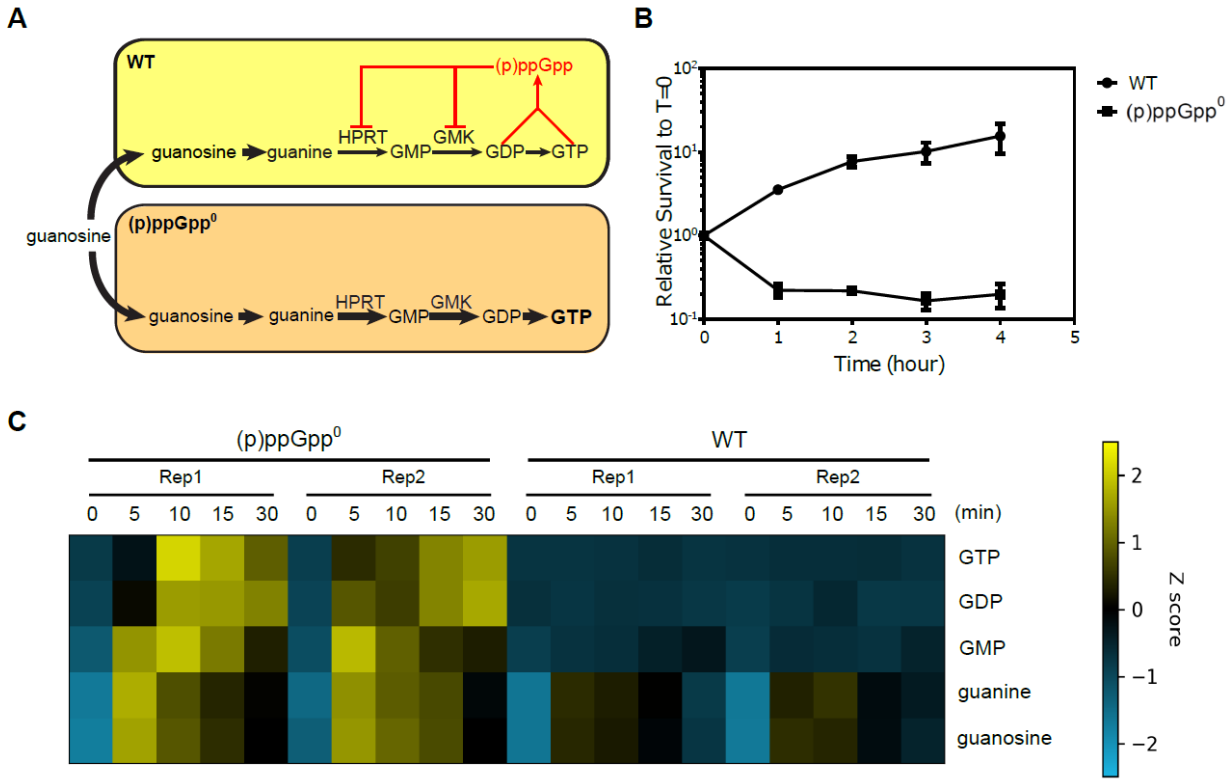

Figure 1. Characterization of guanosine toxicity in (p)ppGpp^0 cells.

(A) Schematic of guanosine utilization in WT and (p)ppGpp^0 cells. GTP biosynthesis is only partially shown here. (B) Guanosine is toxic to (p)ppGpp^0 cells. (C) LC-MS measurement of G nucleosides and nucleotides in WT and (p)ppGpp^0 cells following guanosine treatment.

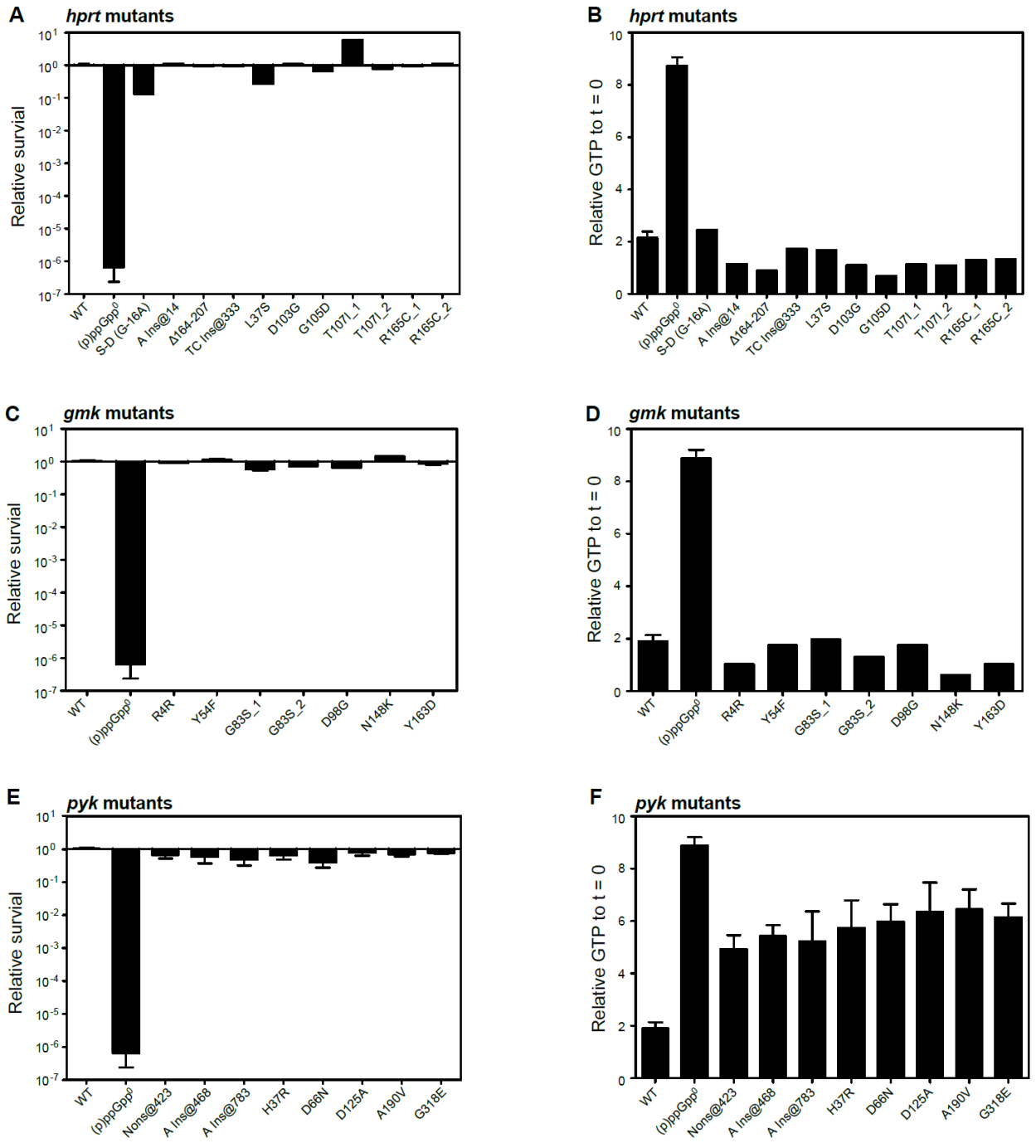

Figure 2. Identification and characterization of *hprt*, *gmk*, and *pyk* mutants.

Plating efficiency of *hprt* mutants (A), *gmk* mutants (C), and *pyk* mutants (E). Plating efficiency = colony forming units (CFUs) with guanosine/ CFUs without guanosine. Change of GTP levels of *hprt* mutants (B), *gmk* mutants (D), and *pyk* mutants (F), following guanosine treatment by thin

layer chromatography (TLC). S-D: Shine- Dalgarno sequence; Ins: insertion; Δ: deletion. The *hprt* T107I _1 and _2 mutants and R165C_1 and _2 mutants, as well as the *gmk* G83S_1 and _2 mutants, were independently identified.

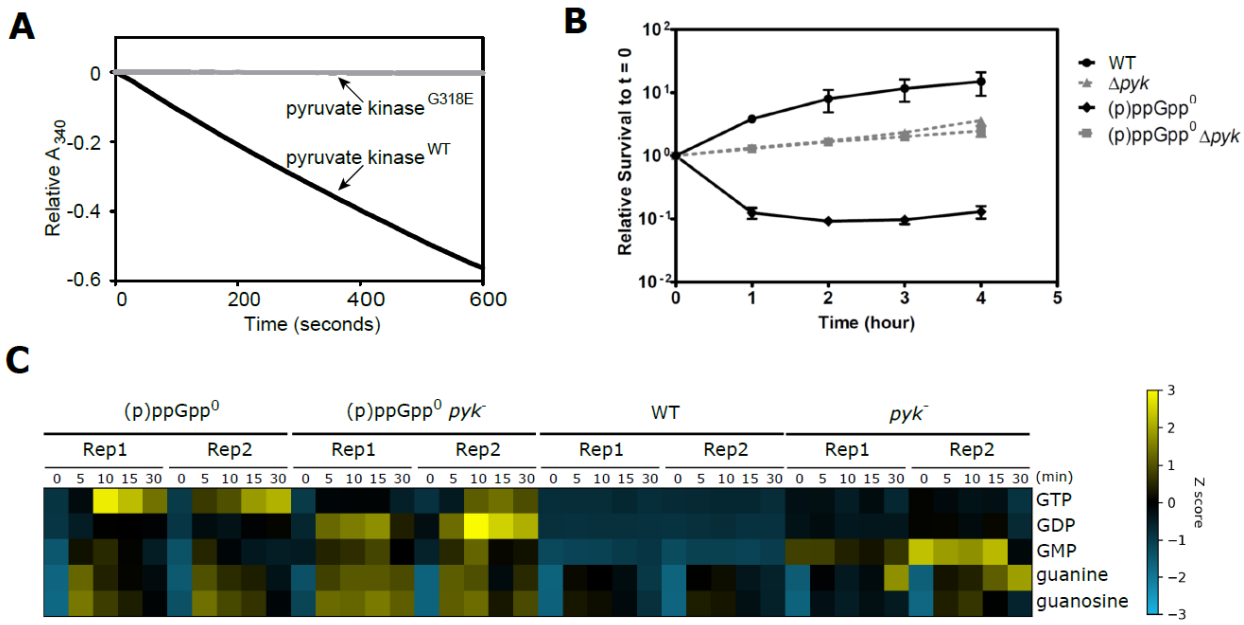

Figure 3. Loss of function mutations in *pyk* rescue guanosine toxicity.

(A) The pyruvate kinase^{G318E} is catalytically inactive. (B) Relative survival after guanosine treatment compared to time 0. (C) Change of G nucleosides and nucleotides in *B. subtilis* strains following guanosine treatment. Data for WT and (p)ppGpp^0 are the same as in Figure 1B, but are shown here for comparison.

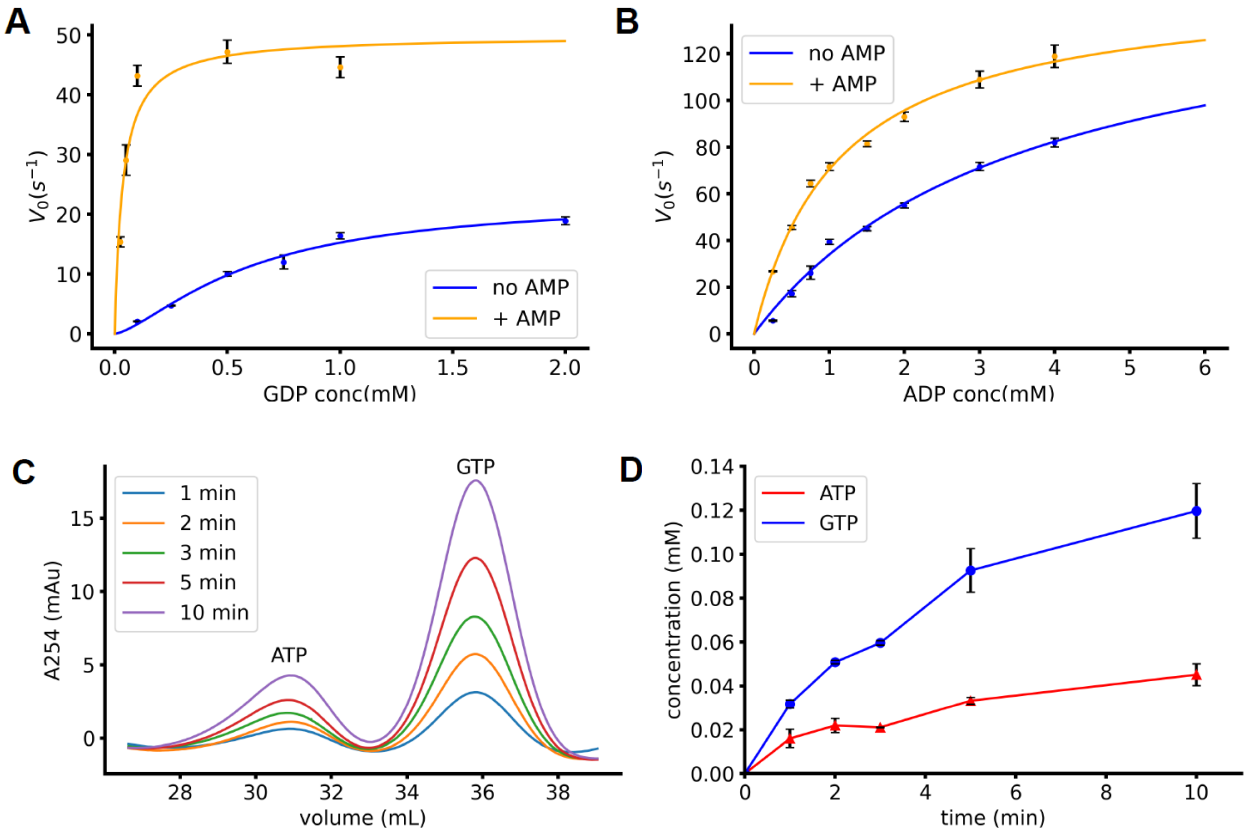

Figure 4. *Bacillus subtilis* pyruvate kinase prefers to produce GTP instead of ATP.

(A) pyruvate kinase kinetics curve with ADP as substrate, with or without 1 mM AMP. (B) pyruvate kinase kinetics curve with GDP as substrate, with or without 1 mM AMP. (C) Amount of products over time in pyruvate kinase reaction with ADP, GDP and AMP at physiological concentrations (0.5 mM, 0.2 mM and 0.1 mM respectively). ATP and GTP are separated with strong anion exchange column, and showed with the absorbance at 254 nm. One out of three replicates are shown here. (D) Quantification of the data in (C) and the other two replicates. Error bars stand for standard error mean for triplicates.

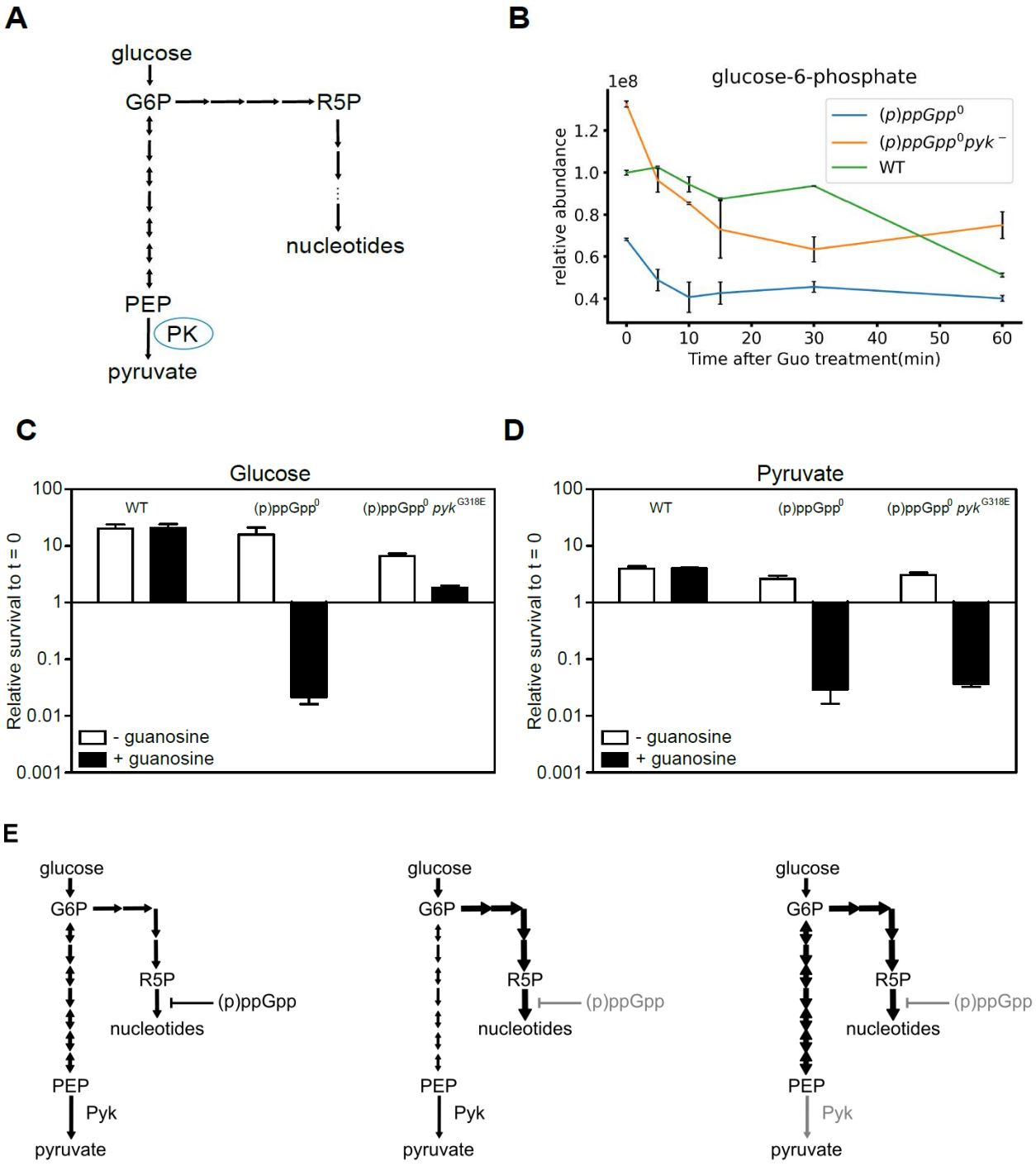

Figure 5. Loss-of-function of pyruvate kinase compensates depletion of glycolysis intermediates

(A) A schematic of the connection between glycolysis and nucleotides synthesis. PK: pyruvate kinase. (B) Change of glucose 6-phosphate level in wild type, (p)ppGpp^0 and (p)ppGpp^0 *pyk*$^-$ cells after guanosine treatment. Survival of wild type, (p)ppGpp^0 and (p)ppGpp^0 *pyk*$^-$ cells grown in (C) glucose media or (D) pyruvate media after guanosine treatment. (E) Schematics of the model that (p)ppGpp regulates the resource partition between nucleotide synthesis and glycolysis, and loss-of-function of pyruvate kinase compensates the depletion of glycolysis intermediates.

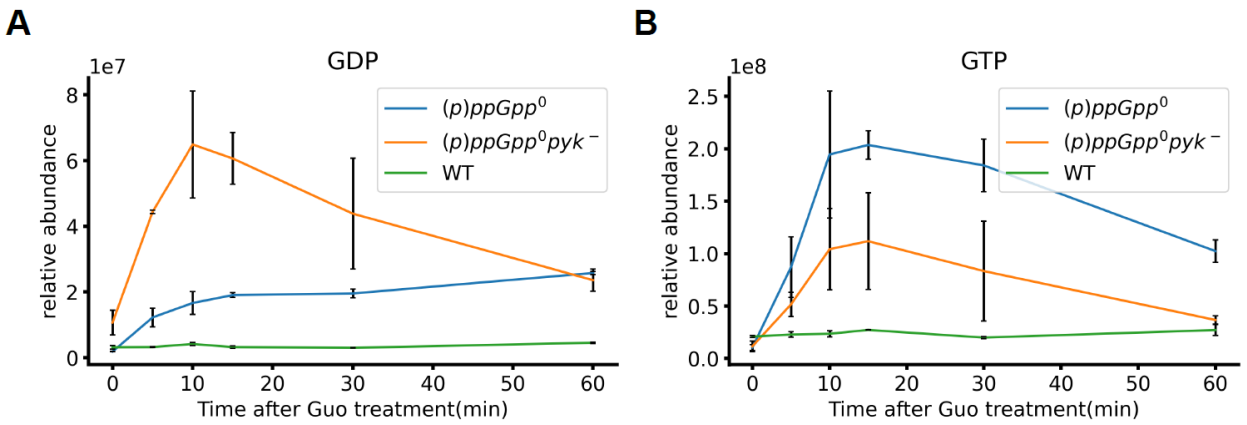

Supplementary Figure 1. Loss-of-function of pyruvate kinase mutation blocks GTP production and leads to accumulation of GDP

(A) GDP level and (B) GTP level in (p)ppGpp^0, (p)ppGpp^0 *pyk*- and WT cells after guanosine treatment.

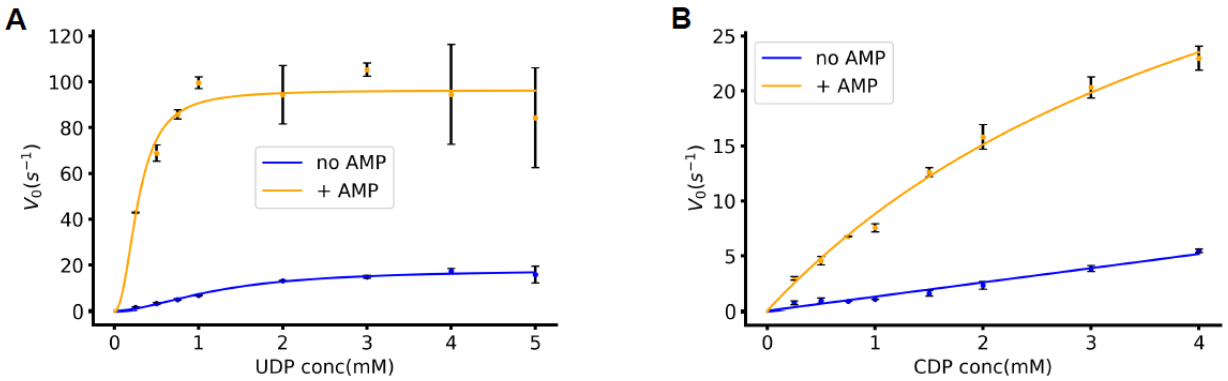

Supplementary Figures 2. *B. subtilis* pyruvate kinase can use UDP and CDP as phosphate acceptor

Pyruvate kinase activity at differemnt concentrations of substrate (A) UDP or (B) CDP.

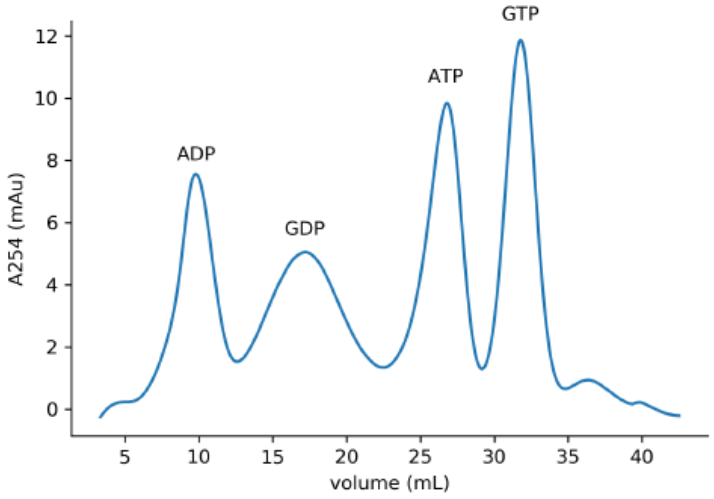

Supplementary Figure 3. Separation of four nucleotide standards with strong anion exchange column

ADP, GDP, ATP and GTP standards can be separated with ion exchange chromatography.

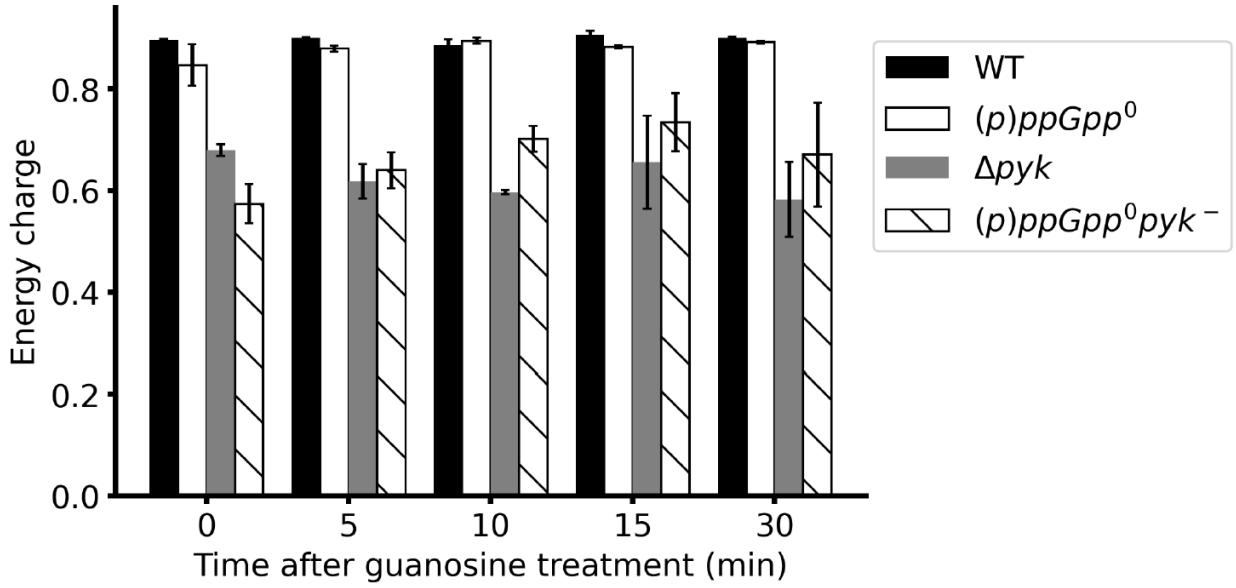

Supplementary Figure 4. Low energy charge in *pyk*⁻ cells may help rescue guanosine toxicity.

Energy charge (energy charge= $\frac{[\mathrm{ATP}]+\frac{1}{2}[\mathrm{ADP}]}{[\mathrm{ATP}]+[\mathrm{ADP}]+[\mathrm{AMP}]}$) in (p)ppGpp^0, (p)ppGpp^0 *pyk*^{G138E}, WT and *Δpyk* cells before and after guanosine treatment.

Chapter 4: Discussion and Future Directions

Different cellular processes are not individual pathways, they usually connect with each other and form a complex network. There are enzymes and compounds involved in multiple pathways to coordinate the network. In my thesis work, I found that the central carbon metabolism enzyme pyruvate kinase contributes significantly to GTP production in nucleotide metabolism. Pyruvate kinase has been reported to have a broad substrate range, but my work showed the physiological effect of promiscuity of pyruvate kinase. I also found that regulation of pyruvate kinase activity controls the resource allocation in central carbon metabolism, especially in gluconeogenesis. It has been proposed long ago that pyruvate kinase needs to be inhibited during gluconeogenesis to avoid a futile cycle[1]. My thesis work showed that in the Gram-positive model organism *B. subtilis,* the futile cycle caused by failure of inhibition of pyruvate kinase does not affect the growth. On the other hand, the inhibition of pyruvate kinase activity during gluconeogenesis is crucial to build up a high PEP level, which is important for synthesizing biosynthetic precursors required for growth. Regulation of pyruvate kinase also affects the susceptibility to antimicrobial reagent that targets metabolism. Glyphosate, the active intergradient of Roundup, inhibits the shikimate pathway by competing with PEP[2]. Inhibition of pyruvate kinase during gluconeogenesis builds up a high PEP level, and leads to much higher resistance to glyphosate.

I. Role of the futile cycle caused by constitutively active pyruvate kinase during gluconeogenesis

Inhibition of pyruvate kinase during gluconeogenesis is usually proposed to avoid the futile cycle between glycolysis and gluconeogenesis. In some bacteria, gluconeogenesis is initiated by direct synthesis of PEP from pyruvate by PEP synthase or pyruvate, phosphate dikinase (PPDK). In other organisms including *B. subtilis*, gluconeogenesis is initiated by synthesis of PEP from OAA. If pyruvate or pyruvate derivatives are the gluconeogenic

substrate, OAA is generated from pyruvate by pyruvate carboxylase. If pyruvate kinase is active during gluconeogenesis, a futile cycle will form among PEP, pyruvate and OAA (Chapter 3 Figure 3). However, when we delete pyruvate carboxylase, we still observed the same growth defect and low growth yield caused by constitutively active pyruvate kinase, indicating that the futile cycle itself did not play an important role.

II. Possible mechanisms of pyruvate kinase inhibition during gluconeogenesis

An open question is how the ECTD of pyruvate kinase helps to inhibit the activity of pyruvate kinase during gluconeogenesis. We found that ECTD is required for the allosteric regulation of pyruvate kinase, but the allosteric effectors concentration change cannot fully explain the almost full inhibition of pyruvate kinase. A possible explanation is that the ECTD is involved in some post-translational modification like phosphorylation that regulates the activity of pyruvate kinase. Another question is: How do other organisms that do not harbor ECTD in their pyruvate kinase inhibit pyruvate kinase activity during gluconeogenesis? It is reported that in yeast pyruvate kinase is inhibited by the depletion of the activator fructose 1,6-bisphosphate concentration. And rat liver pyruvate kinase is inhibited by phosphorylation upon insulin signal. These results indicate that although the sequence of pyruvate kinase is conserved across kingdoms, the subtle structural differences of pyruvate kinase may lead to different modes of regulation of pyruvate kinase. As a highly regulated node in central carbon metabolism, different regulations are evolved to fit different environments and different lifestyles.

III. Possible mechanisms of guanosine toxicity and its suppressors

The detailed mechanism of guanosine toxicity remains unclear. We found that loss-of-function of pyruvate kinase suppressed guanosine toxicity, it could be the result of decreased GTP synthesis from pyruvate kinase, or the compensation of glycolysis intermediates. We noticed that as the concentration of extracellular guanosine concentration increased, the

intracellular GTP level did not increase linearly corresponding to the guanosine concentration. In contrast, GTP level increased suddenly at a certain guanosine concentration, as if there was positive feedback in uptake of guanosine or the synthesis of GTP. On the other hand, we also found that the killing caused by guanosine also had a threshold, indicating that there may be a switch-like regulation in GTP synthesis. High GTP might kill cells by inserting into DNA and cause DNA damage.

No suppressor mutations were found in the *ndk* gene that encodes nucleoside diphosphate kinase (NDK). NDK converts dNDPs and NDPs to dNTPs and NTPs, respectively, but loss of *ndk* was not lethal[3], suggesting the existence of alternative pathways to produce nucleoside triphosphates. Given the broad substrate range of pyruvate kinase, we wonder whether pyruvate kinase plays the role of NDK in *ndk*$^-$ cells. Intriguingly, *pyk*$^-$ *ndk*$^-$ double mutant can form colonies similar to *pyk*$^-$. (Data not shown). This indicates there are still other enzymes with the same function. It has been reported in *E. coli* that adenylate kinase (*adk*) is responsible for the residue NDK activity[4], but we cannot test the viability of *ndk*$^-$ *adk*$^-$ directly because *adk* is essential.

IV. Final perspectives

Bacteria possess many different metabolic pathways compared to humans, which provides many valuable drug targets. The famous herbicide glyphosate targets shikimate pathway, which is found in bacteria, fungi, and plants, but absent in animals. It inhibits the growth of bacteria as well as plants. Using glyphosate as an example, we found that the regulation of pyruvate kinase affects the resistance to glyphosate significantly. This brings up the idea that antimicrobial reagents can be used together with compounds that manipulate the metabolism of microorganisms to increase the sensitivity.

Many biochemical reactions are going on in a tiny cell simultaneously, complex regulations are required to coordinate the metabolic network. My thesis work focuses on a central carbon metabolism enzyme pyruvate kinase, providing experimental evidence for the physiological impact of loss of pyruvate kinase activity or constitutive pyruvate kinase activity. This provides an example of how one enzyme can connect nucleotide metabolism, central carbon metabolism and drug resistance.

Reference

1. Hers, H. G. & Hue, L. Gluconeogenesis and related aspects of glycolysis. *Annu. Rev. Biochem.* **52**, 617–653 (1983).

2. Steinrücken, H. C. & Amrhein, N. The herbicide glyphosate is a potent inhibitor of 5-enolpyruvyl-shikimic acid-3-phosphate synthase. *Biochem. Biophys. Res. Commun.* **94**, 1207–1212 (1980).

3. Kobayashi, K. *et al.* Essential Bacillus subtilis genes. *Proc. Natl. Acad. Sci. U. S. A.* **100**, 4678–4683 (2003).

4. Lu, Q. & Inouye, M. Adenylate kinase complements nucleoside diphosphate kinase deficiency in nucleotide metabolism. *Proc. Natl. Acad. Sci. U. S. A.* **93**, 5720–5725 (1996).

Appendix I: Development of a microfluidic device suitable for real time biofilm imaging under treatment

Introduction

In contrast to planktonic cultures grown in laboratory flasks, bacteria often thrive in complex communities known as biofilms in various natural environments[1]. Within a genetically homogeneous biofilm, remarkable phenotypic heterogeneities are frequently observed[2]. To study the complex system, fluorescence microscopy is usually applied to visualize various signals from different cells.

Biofilms are either adherent colonies on solid interfaces or as floating structures at the liquid-air interface, commonly referred to as pellicles[3]. To visualize live biofilms under microscope, a common approach is imaging the biofilm on a small agar piece or within the wells of a plate, particularly in the case of pellicles. Nevertheless, these existing methods are limited in monitoring the response of a biofilm to various treatments. In light of this, we have developed a microfluidic device that enables real-time imaging of live biofilms while offering the ability to change media without disturbing the integrity of the biofilm.

Methods

Microfluidic device design and Biofilm imaging

Microfluidic device mold is fabricated from a glass microscope slide (3 inches X 2 inches), both faces of the slide are siliconized to reduce the stickiness to polydimethylsiloxane (PDMS). A piece of Scotch™ tape is taped on the siliconized face, and then is cut into the shape of channel (10 mm X 1 mm) and chamber (20 mm X 5 mm, for biofilm growth). To keep the semipermeable membrane from touching the slide, several squares of the scotch tape are left

alongside the chamber and channel. Four corners of the slide are polished by sandpapers to avoid cutting the aluminum foil. The slide is wrapped by a piece of aluminum foil into bowl shape as the container of PDMS, make sure it is not leaky. A piece of semipermeable membrane (from dialysis tube) is put on the top of the chamber, and aligned to the tape to cover the whole chamber and partial channels.

A small block of rectangular cuboid metal on the top center of the membrane. Other heat-tolerant high thermal conductivity materials should work as well. PDMS is mixed with curing agent and poured on the top of the mold. The whole system is degassed for 15 min, make sure no bubble left after degassing. PDMS is solidified at 100 °C overnight.

After the PDMS is solidified, remove the aluminum foil carefully. Then cut the device out fitting the size of coverslip. Remove the thin layer of PDMS on the top and bottom of the exposed semipermeable membrane, clean both faces of the exposed membrane with hexane to make it clear. The solidified device is processed by punching holes for inlet and outlet at the end of each channel. The bottom of the device is plasma-treated to covalently bind to coverslip for imaging.

The flow can be controlled by gravity or syringe pumps, syringe pumps are highly recommended because stable pressure can keep the membrane in focus. Media is flowed through the bottom of the membrane and bacteria are inoculated on the top of the membrane. Biofilm will form on the top of the membrane.

Result

The development of *Bacillus subtilis* NCIB3610 biofilm was recorded using the microfluid device as an example. P_{ilvB}-*mCherry* P_{rrnB}-*sfGFP* double reporter are incorporated into the genome of *B. subtilis* as indicators of growth. In actively growing cells, P_{rrnB} is highly active due to the demand of ribosome synthesis. In stressed/slow growing cells, P_{ilvB} is highly active

because low GTP level relives the repression of P_{ilvB} by CodY. Therefore, fast growing cells will be green and slowing growing cells will be red. We observed that virtually all cells were fast growing initially (Figure 1). When cells were getting crowded and starting chaining, nematic patterns were observed (Figure 1), agreeing with previous reports in other systhems[4,5]. In the later growth stage, we observed that cells expanding at the edge stayed actively growing, while the cells in the center of the biofilm started to slow down growth (Figure 1).

The novel function of our microfluidic device is that it allows real-time imaging of biofilm under treatment without disrupting the biofilm. Using this function, we monitored the response of *B. subtilis* biofilm to a short-term treatment of antibiotic ciprofloxacin. We observed shut down of cell growth after ciprofloxacin treatment, followed by lysis of most cells (Figure 2). After removal of ciprofloxacin, cells were able to regrow in 24 hours, indicating the loss of inhibition and killing from ciprofloxacin.

Discussion

Biofilm is a structure formed by microbial cells and the extracellular matrix produced by the cells. Biofilm is widely studied because it is associated with antibiotic tolerance. Nonetheless, current biofilm imaging methods are hard to monitor the response of live biofilm to antibiotic treatment without disrupting the structure of biofilm. Here we developed a new microfluidic device, in which the biofilm grows on the top of a semipermeable membrane, while the media flows beneath the membrane and the nutrition diffuses to the top of the membrane to support biofilm growth. Thus, switching media will not disrupt the structure of the biofilm. Using this biofilm growth and imaging device, we observed the nematic patterns of biofilm formed by chaining bacteria, and monitored the killing and recovery of biofilm after antibiotic ciprofloxacin treatment and removal, showing the potential of our microfluidic device in real-time live biofilm imaging under treatment of interest.

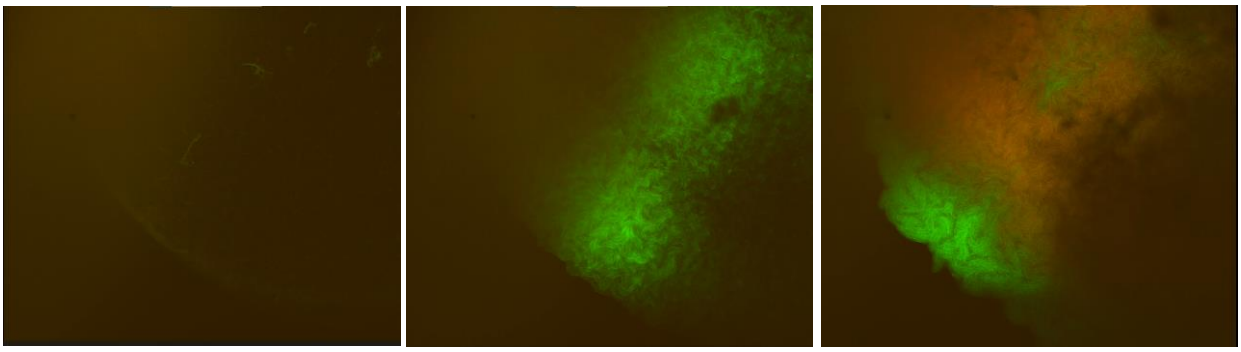

Figure 1. Biofilm formation on the microfluidic device

The biofilm development of *B. subtilis* NCIB3610 with P_{ilvB}-*mCherry* P_{rrnB}-*sfGFP* double reporter.

Left: 0 hour after inoculation; Middle: 3 hour after inoculation; Right: 6 hours after inoculation.

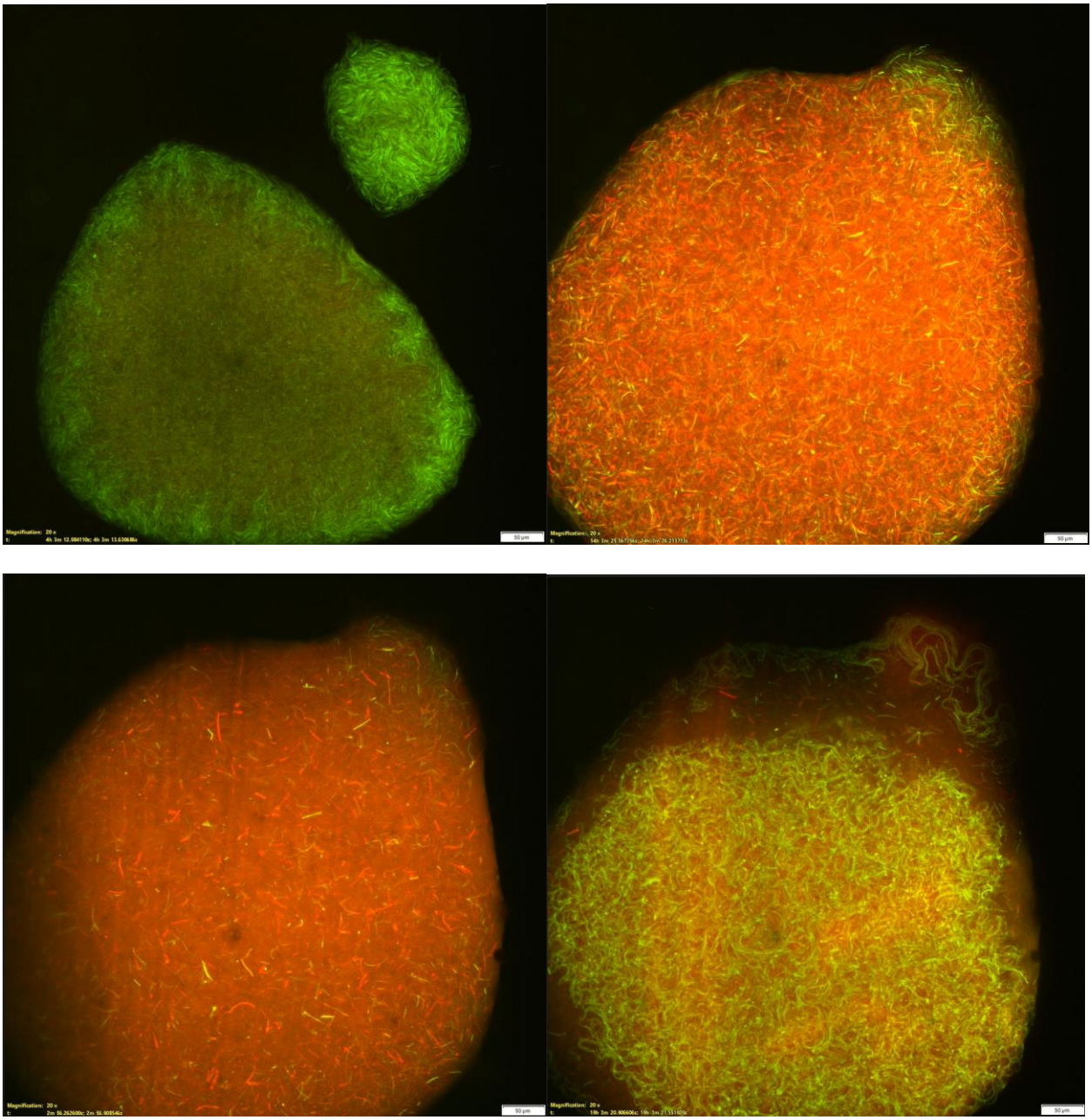

Figure 2. Response of biofilm to short-term antibiotic treatment

The biofilm of *B. subtilis* NCIB3610 with P_{ilvB}-*mCherry* P_{rrnB}-*sfGFP* double reporter were treated by ciprofloxacin for 20 hours followed by removal of ciprofloxacin and 24 hours growth. Top left: 0 hour after ciprofloxacin treatment; Top right: 10 hours after ciprofloxacin treatment; Bottom left: 0 hour after ciprofloxacin removal; Bottom right: 19 hours after ciprofloxacin removal.

Reference

1. O'Toole, G., Kaplan, H. B. & Kolter, R. Biofilm formation as microbial development. *Annu. Rev. Microbiol.* **54**, 49–79 (2000).

2. Stewart, P. S. & Franklin, M. J. Physiological heterogeneity in biofilms. *Nat. Rev. Microbiol.* **6**, 199–210 (2008).

3. Branda, S. S., González-Pastor, J. E., Ben-Yehuda, S., Losick, R. & Kolter, R. Fruiting body formation by Bacillus subtilis. *Proc. Natl. Acad. Sci. U. S. A.* **98**, 11621–11626 (2001).

4. Zhang, Q. *et al.* Morphogenesis and cell ordering in confined bacterial biofilms. *Proc. Natl. Acad. Sci. U. S. A.* **118**, (2021).

5. Yaman, Y. I., Demir, E., Vetter, R. & Kocabas, A. Emergence of active nematics in chaining bacterial biofilms. *Nat. Commun.* **10**, 2285 (2019).